Monthly Notices
of the
ROYAL ASTRONOMICAL SOCIETY

Mon. Not. R. Astron. Soc. **408,** 1147–1167 (2010) doi:10.1111/j.1365-2966.2010.17196.x

First CCD *UBVI* photometric analysis of four moderately young open clusters in the third galactic quadrant

Andrés E. Piatti,[1⋆] Juan J. Clariá[2⋆] and Andrea V. Ahumada[2,3⋆]

[1]*Instituto de Astronomía y Física del Espacio, CC 67, Suc. 28, 1428 Ciudad de Buenos Aires, Argentina*
[2]*Observatorio Astronómico, Universidad Nacional de Córdoba, Laprida 854, 5000 Córdoba, Argentina*
[3]*European Southern Observatory, Alonso de Córdova 3107, Santiago, Chile*

Accepted 2010 June 11. Received 2010 June 11; in original form 2010 April 14

ABSTRACT

We present CCD photometry in the Johnson *UBV* and Kron–Cousins *I* systems down to $V \sim 22.0$ for the open clusters NGC 2311, Trumpler 6, NGC 2432 and BH 54 and their surrounding fields. Trumpler 6 and BH 54 have never been studied before and so we provide, for the first time, estimates of their fundamental parameters. We obtained colour–magnitude diagrams (CMDs) and colour–colour diagrams cleaned from field star contamination by statistically subtracting stars in terms of spatial density, magnitude and colour distributions. Cluster angular radii were estimated from star counts in appropriate-sized boxes distributed throughout the entire observed fields. Using the cleaned CMDs and colour–colour diagrams, we applied sound photometric membership criteria to discriminate cluster members from interloper field stars. The interstellar extinction across the cluster fields derived from the 100-μm dust emission full-sky maps can be considered uniform within the quoted uncertainties. The $E(B-V)$ and $E(V-I)$ colour excesses and the apparent distance moduli of the clusters were estimated from the fit of the zero-age main-sequence to the colour–colour diagrams and CMDs, respectively. Cluster ages were determined from the comparison of the four clusters' CMDs with solar metallicity theoretical isochrones of the Geneva group. All the clusters were found to be moderately young objects, their ages ranging between 60 and 250 Myr.

Key words: techniques: photometric – open clusters and associations: general – open clusters and associations: individual: NGC 2311 – open clusters and associations: individual: Trumpler 6 – open clusters and associations: individual: NGC 2432 – open clusters and associations: individual: BH 54.

1 INTRODUCTION

Open clusters (OCs) are formed in the Galactic disc and are distributed throughout it. They are ideal objects for focusing on several astrophysical problems, such as star formation, stellar evolution and dynamic evolution of stellar systems (see e.g. Bonatto & Bica 2005, and references therein) as well as chemical evolution of the Galactic disc (see e.g. Hou, Chang & Chen 2002, and references therein). The OCs happen to be ideal due to the fact that they are self-gravitating groups of stars spanning a wide mass range, located at the same distance, which were formed under the same conditions and approximately at the same time. These properties allow OC distances and ages to be more easily and accurately determined than other disc objects. However, the proximity of most OCs to the Galactic plane and their corresponding high reddening values and field star contaminations have restricted OC studies to the most populous ones and/or to those located a few kpc far from the Sun.

According to the recently updated version (2009 February) of the Dias et al.'s (2002, http://www.astro.iag.usp.br/wilton) OC catalogue, 1787 OCs are suspected to exist in the Milky Way disc. These are excellent objects to probe the structure and evolution of the Galactic disc (Janes & Phelps 1994; Friel 1995; Bonatto et al. 2006; Piskunov et al. 2006). Unfortunately, fundamental parameters like distances, reddenings and ages are available for fewer than half of the OCs in this sample. All we know about the majority of the catalogued OCs are their positions and approximate angular sizes, which are inaccurate in many cases (Archinal & Hynes 2003). Moreover, since most of the unstudied OCs are classified as Trumpler class *p* objects (Trumpler 1930), our current knowledge of OCs is considered to be heavily biased by the properties of rich clusters. To examine, for example, how the disc properties evolved in time, we must improve the statistics of well-studied OCs. In fact, the greater the number of OCs with well determined distances, the more accurate and detailed the analysis of the structure and the metal

⋆E-mail: andres@iafe.uba.ar (AEP); claria@oac.uncor.edu (JJC); aahumada@eso.org (AVA)

Table 1. Basic parameters of the four studied OCs.

Cluster	α_{2000} ($^{h}\,^{m}\,^{s}$)	δ_{2000} ($^{\circ}\,'\,''$)	l ($^{\circ}$)	b ($^{\circ}$)	Trumpler class	Angular diameter (arcmin)	Number of measured stars	Number of inferred cluster stars
NGC 2311	06 57 47	−04 36 42	217.76	−0.69	III-2m	6.0	945	50
Trumpler 6	07 26 25	−24 12 00	238.33	−3.64	III-2p	6.0	3391	20
NGC 2432	07 40 53	−19 04 36	235.47	+1.78	II-2m	6.0	3459	28
BH 54	08 49 41	−44 22 00	264.48	−0.28	II-1p	4.0	800	13

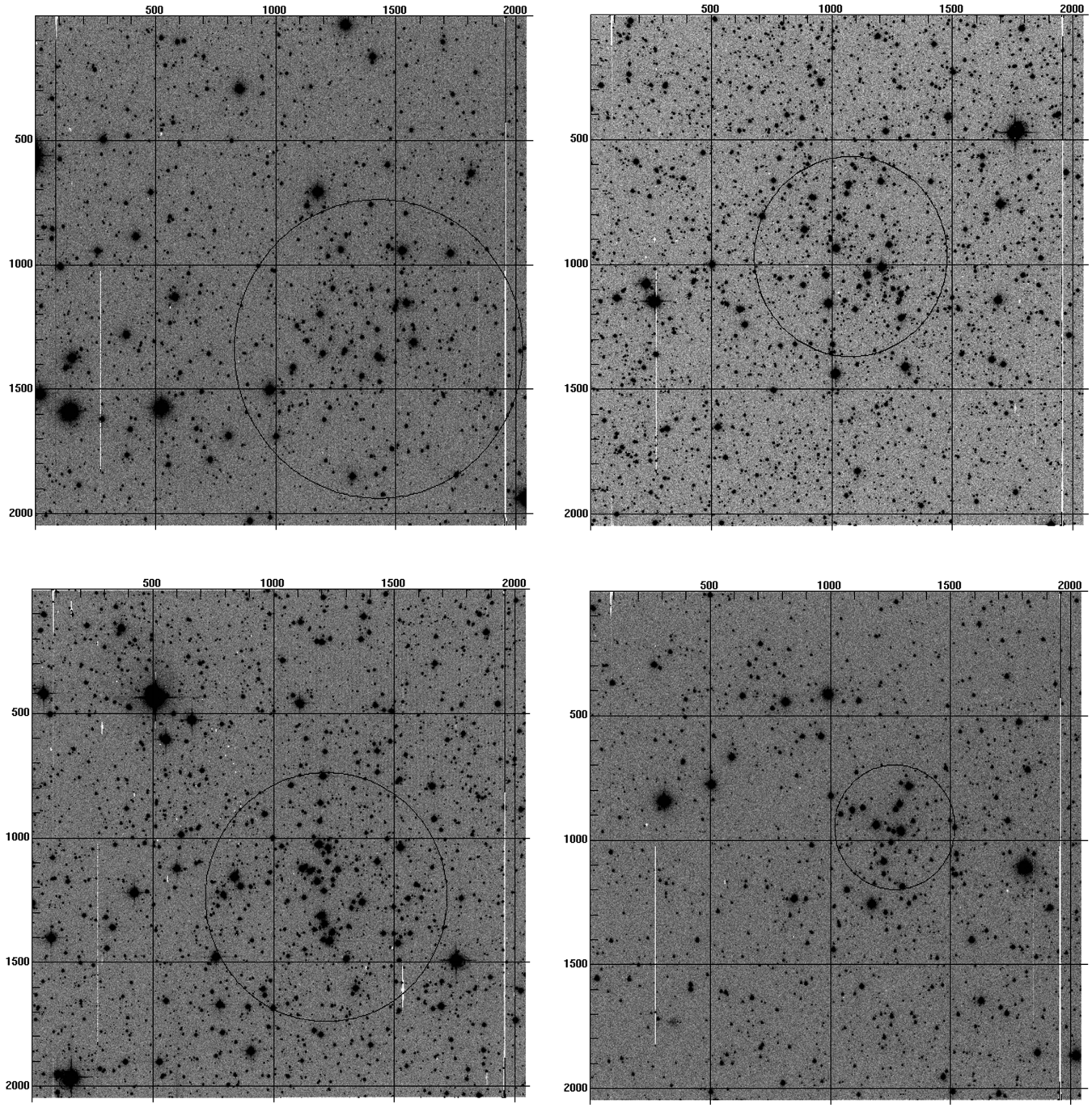

Figure 1. Deepest CCD images obtained: 90 s *I* for NGC 2311 (top left); 200 s *V* for Trumpler 6 (top right); 200 s *V* for NGC 2432 (bottom left) and 90 s *I* for BH 54 (bottom right). Coordinates are given in pixels. North is up and east is to the left. The circles centred on $(x_c, y_c) = (1430,1340)$, (1080,970), (1220,1240) and (1270,950) pixels encompass the NGC 2311, Trumpler 6, NGC 2432 and BH 54 regions, respectively.

abundance gradient in the Galactic disc as well as their evolution over time.

The photometric data reported in this study were obtained as part of a project still under development aimed at obtaining the basic parameters of some unstudied OCs and at refining the quality of observationally determined properties for some poorly studied ones. Reliable basic astrophysical properties of unstudied OCs are important both to carry on disc studies and to constrain theories of molecular cloud fragmentation, star formation, as well as stellar and dynamical evolution. Structural and dynamical related parameters of OCs can be used to examine whether the apparent scarcity of OCs inside the solar circle is due to observational limitations in dense stellar fields or to enhanced tidal disruption rates because of their proximity to the bulge and/or to higher rates of collisions with molecular clouds (Bonatto et al. 2006, and references therein).

We report here the results obtained from CCD $UBVI_{\rm KC}$ photometry up to $V \leq 21.0$ in the fields of the selected OCs NGC 2311, Trumpler 6, NGC 2432 and BH 54. These are low Galactic-latitude OCs ($|b| \leq 3\overset{\circ}{.}7$) located at the third Galactic quadrant. Their basic parameters are given in Table 1, where Trumpler class was taken from Archinal & Hynes (2003). The last two columns list the total number of measured stars in this study and the total number of stars inferred as cluster members. A brief description of these OCs is given below.

NGC 2311. Also referred to as Collinder 123 (Collinder 1931) or C0655−045, this is a detached cluster in Monoceros with little central concentration and medium range in the brightness of the stars (Fig. 1). Lyngå (1987) reported an angular diameter of 7 arcmin. Although Moitinho (2001) obtained CCD *UBVRI* photometry for NGC 2311, he did not derive the cluster's parameters. More recently, Kharchenko et al. (2005) presented a catalogue of astrophysical data of 520 Galactic OCs – among them NGC 2311 – which could be identified in the All-Sky Compiled Catalogue (ASCC-2.5; Kharchenko 2001). By applying homogeneous methods and algorithms, Kharchenko et al. (2005) determined basic parameters for their cluster sample. For NGC 2311, they found the following results: $E(B-V) = 0.20$, $d = 2.0$ kpc and $t \sim 400$ Myr. However, we should be cautious when considering these findings since the limiting magnitude of the ASCC-2.5 is $V \approx 12.5$. In a preliminary study, Ahumada, Clariá & Bica (2007) determined $E(B-V) = 0.15$ and estimated an age within the (200–350) Myr range from a flux-calibrated integrated spectrum of NGC 2311.

Trumpler 6. Also known as Collinder 145 (Collinder 1931) or C0742−242, this object has been classified as a Trumpler (1930) class III-2p system in Canis Major, i.e. a poor, detached cluster without noticeable central concentration and a medium range in the brightness of the stars (Fig. 1). According to Lyngå (1987), its angular diameter is about 6 arcmin. No parameters are currently available for this cluster in the WEBDA Open Cluster Database (Mermilliod & Paunzen 2003).

NGC 2432. This is a Puppis cluster also designated as Collinder 157 (Collinder 1931), Melotte 73 (Melotte 1915) or C0738−189. Archinal & Hynes (2003) refer to this cluster as belonging to Trumpler class II-2m, i.e. a moderately rich, detached cluster with little central concentration and medium-range bright stars (Fig. 1). Old distance determinations range from 1.1 to 3.1 kpc (Alter, Ruprecht & Vanisek 1970), although most recent evidence places NGC 2432 at ∼2.0 kpc (Kharchenko et al. 2005). NGC 2432 has a relatively small angular diameter of about 7 arcmin (Lyngå 1987). Even when this feature renders it appropriate for CCD camera observations, the only CCD photometric study up to date was performed by Kharchenko et al. (2005), who derived $E(B-V) = 0.12$, $d = 2.03$ kpc and an age of ∼150 Myr. As for NGC 2311, Moitinho (2001) obtained *UBVRI* photometry for NGC 2432 but he did not derive the cluster's parameters.

BH 54. This is a detached, moderately poor OC in Vela in which most of the stars exhibit nearly the same apparent brightness (Fig. 1). BH 54 has a small angular diameter of 4 arcmin (Lyngå 1987). As far as we are aware, no previous data exist for this small-sized object first recognized as an OC by van den Bergh & Hagen (1975).

This paper is organized as follows: in Section 2, we briefly describe the observations, the data reduction process and the quality of the photometric data. In Section 3, we present the observed colour–magnitude diagrams (CMDs) and colour–colour diagrams and we explain how to minimize the field star contamination. We also determine the cluster centres and stellar density radial profiles. In Section 4, we apply two sound photometric criteria to discriminate cluster members and we examine the interstellar reddening across the observed fields. Section 5 deals with the determination

Table 2. Observation log of studied clusters.

Cluster	Date	Filter	Exposure (s)	Airmass	Seeing (arcsec)
NGC 2311	2000 December 25	*V*	20	1.16	1.2
		V	60	1.14	1.2
		V	200	1.13	1.3
		B	20	1.13	1.0
		B	60	1.13	1.0
		B	360	1.13	1.2
		I	10	1.12	1.1
		I	90	1.12	1.1
		U	60	1.12	1.1
		U	540	1.12	1.3
Trumpler 6	2000 December 27	*U*	60	1.21	1.2
		U	540	1.19	1.5
		B	20	1.16	1.3
		B	60	1.15	1.3
		B	360	1.15	1.4
		V	20	1.14	1.3
		V	60	1.13	1.3
		V	200	1.13	1.3
		I	10	1.12	1.1
		I	90	1.11	1.2
NGC 2432	2000 December 29	*U*	60	1.21	1.2
		U	540	1.19	1.2
		B	540	1.16	1.4
		B	20	1.15	1.3
		B	60	1.15	1.3
		B	180	1.14	1.3
		V	20	1.13	1.3
		V	60	1.13	1.3
		V	60	1.12	1.1
		V	200	1.11	1.2
		I	10	1.11	1.2
		I	10	1.10	1.3
		I	90	1.10	1.3
BH 54	2000 December 25	*V*	20	1.21	1.2
		V	60	1.19	1.2
		V	200	1.16	1.2
		B	360	1.15	1.2
		B	60	1.15	1.2
		B	20	1.14	1.2
		I	10	1.13	1.1
		I	90	1.13	1.3
		U	60	1.12	1.1
		U	540	1.11	1.5

Table 3. Resulting coefficients for the transformation equations.

Instrumental magnitude	Night	a	b	c	Colour	rms errors
u	December 25	3.777 ± 0.021	0.434 ± 0.013	-0.068 ± 0.008	$U-B$	0.027
	December 27	3.768 ± 0.055	0.425 ± 0.039	-0.014 ± 0.013	$U-B$	0.057
	December 29	4.485 ± 0.078	0.491 ± 0.061	-0.059 ± 0.014	$U-B$	0.054
b	December 25	2.102 ± 0.022	0.218 ± 0.015	0.128 ± 0.008	$B-V$	0.026
	December 27	2.096 ± 0.027	0.248 ± 0.018	0.101 ± 0.008	$B-V$	0.029
	December 29	2.859 ± 0.031	0.262 ± 0.023	0.104 ± 0.006	$B-V$	0.020
v	December 25	1.952 ± 0.017	0.112 ± 0.011	-0.010 ± 0.007	$B-V$	0.025
		1.962 ± 0.016	0.109 ± 0.010	-0.013 ± 0.006	$V-I$	0.022
	December 27	1.933 ± 0.012	0.144 ± 0.008	-0.026 ± 0.003	$B-V$	0.012
		1.930 ± 0.017	0.140 ± 0.012	-0.019 ± 0.004	$V-I$	0.019
	December 29	2.701 ± 0.017	0.150 ± 0.013	-0.025 ± 0.004	$B-V$	0.010
		2.695 ± 0.018	0.153 ± 0.015	-0.020 ± 0.003	$V-I$	0.011
i	December 25	2.844 ± 0.023	0.058 ± 0.013	0.023 ± 0.010	$V-I$	0.033
	December 27	2.863 ± 0.023	0.081 ± 0.016	-0.014 ± 0.005	$V-I$	0.022
	December 29	3.588 ± 0.035	0.121 ± 0.028	-0.008 ± 0.007	$V-I$	0.022

Table 4. CCD *UBVI* data for stars in the field of NGC 2311. Only a portion of the table is shown here for guidance regarding its form and content. The full table is available in the online version of the journal (see Supporting Information).

ID	x (pixel)	y (pixel)	V (mag)	$\sigma(V)$ (mag)	n_V	$U-B$ (mag)	$\sigma(U-B)$ (mag)	n_{UB}	$B-V$ (mag)	$\sigma(B-V)$ (mag)	n_{BV}	$V-I$ (mag)	$\sigma(V-I)$ (mag)	n_{VI}
–	–	–	–	–	–	–	–	–	–	–	–	–	–	–
87	168.107	316.505	17.824	0.050	3	0.493	0.059	3	1.066	0.039	3	1.342	0.045	3
88	173.222	1355.202	18.135	0.020	3	0.856	0.004	2	1.286	0.011	2	1.541	0.033	3
89	173.450	973.752	15.567	0.006	3	0.498	0.026	3	0.867	0.009	3	0.879	0.007	3
–	–	–	–	–	–	–	–	–	–	–	–	–	–	–

Note. (x, y) coordinates correspond to the reference system in Fig. 1. Magnitude and colour errors are the standard deviations of the mean, or the observed photometric errors for stars with only one measurement.

Table 5. CCD *UBVI* data for stars in the field of Trumpler 6. Only a portion of the table is shown here for guidance regarding its form and content. The full table is available in the online version of the journal (see Supporting Information).

ID	x (pixel)	y (pixel)	V (mag)	$\sigma(V)$ (mag)	n_V	$U-B$ (mag)	$\sigma(U-B)$ (mag)	n_{UB}	$B-V$ (mag)	$\sigma(B-V)$ (mag)	n_{BV}	$V-I$ (mag)	$\sigma(V-I)$ (mag)	n_{VI}
–	–	–	–	–	–	–	–	–	–	–	–	–	–	–
1750	649.788	1680.575	15.881	0.014	3	1.632	0.048	2	1.416	0.007	2	1.481	0.021	3
1751	664.269	1174.330	18.765	0.029	3	1.304	0.021	2	1.570	0.009	3	1.630	0.012	3
1752	1143.035	1460.944	18.891	0.039	3	1.431	0.013	2	1.587	0.068	3	1.759	0.028	3
–	–	–	–	–	–	–	–	–	–	–	–	–	–	–

Note. (x, y) coordinates correspond to the reference system in Fig. 1. Magnitude and colour errors are the standard deviations of the mean, or the observed photometric errors for stars with only one measurement.

Table 6. CCD *UBVI* data for stars in the field of NGC 2432. Only a portion of the table is shown here for guidance regarding its form and content. The full table is available in the online version of the journal (see Supporting Information).

ID	x (pixel)	y (pixel)	V (mag)	$\sigma(V)$ (mag)	n_V	$U-B$ (mag)	$\sigma(U-B)$ (mag)	n_{UB}	$B-V$ (mag)	$\sigma(B-V)$ (mag)	n_{BV}	$V-I$ (mag)	$\sigma(V-I)$ (mag)	n_{VI}
–	–	–	–	–	–	–	–	–	–	–	–	–	–	–
1441	634.742	880.536	15.428	0.008	4	0.288	0.013	3	0.752	0.005	3	0.847	0.020	4
1442	392.480	880.559	14.193	0.008	4	0.314	0.014	3	0.492	0.003	3	0.589	0.019	4
1443	280.363	880.958	16.938	0.010	4	0.819	0.012	3	1.022	0.005	3	1.117	0.017	4
–	–	–	–	–	–	–	–	–	–	–	–	–	–	–

Note. (x, y) coordinates correspond to the reference system in Fig. 1. Magnitude and colour errors are the standard deviations of the mean, or the observed photometric errors for stars with only one measurement.

of cluster fundamental parameters through the fitting of theoretical isochrones. A comparison of the current cluster results with previous ones is presented in Section 6. Finally, Section 7 summarizes our main findings and conclusions.

2 DATA COLLECTION AND REDUCTION

We obtained images for the cluster sample on the nights of 2000 December 25, 27 and 29 with the $UBVI_{KC}$ filters and a 2048 × 2048 pixel Tektronix CCD attached to the 0.9-m telescope (scale 0.4 arcsec pixel^{-1}) at Cerro Tololo Inter-American Observatory (CTIO), Chile. Its field of view is 13.6 × 13.6 arcmin^2. At the beginning of each observing night, we obtained a series of bias and dome and sky flat-field exposures per filter to calibrate the CCD instrumental signature. In order to standardize our photometry, we carried out observations of standard stars of the selected areas PG 0231+051, 92 and 98 of Landolt (1992). The chosen standard stars cover a wide colour range ($-0.30 < B - V < 2.20$).

Table 7. CCD *UBVI* data for stars in the field of BH 54. Only a portion of the table is shown here for guidance regarding its form and content. The full table is available in the online version of the journal (see Supporting Information).

ID	x (pixel)	y (pixel)	V (mag)	$\sigma(V)$ (mag)	n_V	$U-B$ (mag)	$\sigma(U-B)$ (mag)	n_{UB}	$B-V$ (mag)	$\sigma(B-V)$ (mag)	n_{BV}	$V-I$ (mag)	$\sigma(V-I)$ (mag)	n_{VI}
–	–	–	–	–	–	–	–	–	–	–	–	–	–	–
9	1221.580	1084.344	12.969	0.009	3	0.037	0.013	3	0.658	0.003	3	0.909	0.024	3
10	504.297	774.619	11.364	0.029	2	0.065	0.035	2	0.352	0.012	2	0.456	0.014	2
11	264.369	293.332	12.976	0.007	3	0.073	0.034	3	0.625	0.038	3	0.633	0.009	3
–	–	–	–	–	–	–	–	–	–	–	–	–	–	–

Note. (x, y) coordinates correspond to the reference system in Fig. 1. Magnitude and colour errors are the standard deviations of the mean, or the observed photometric errors for stars with only one measurement.

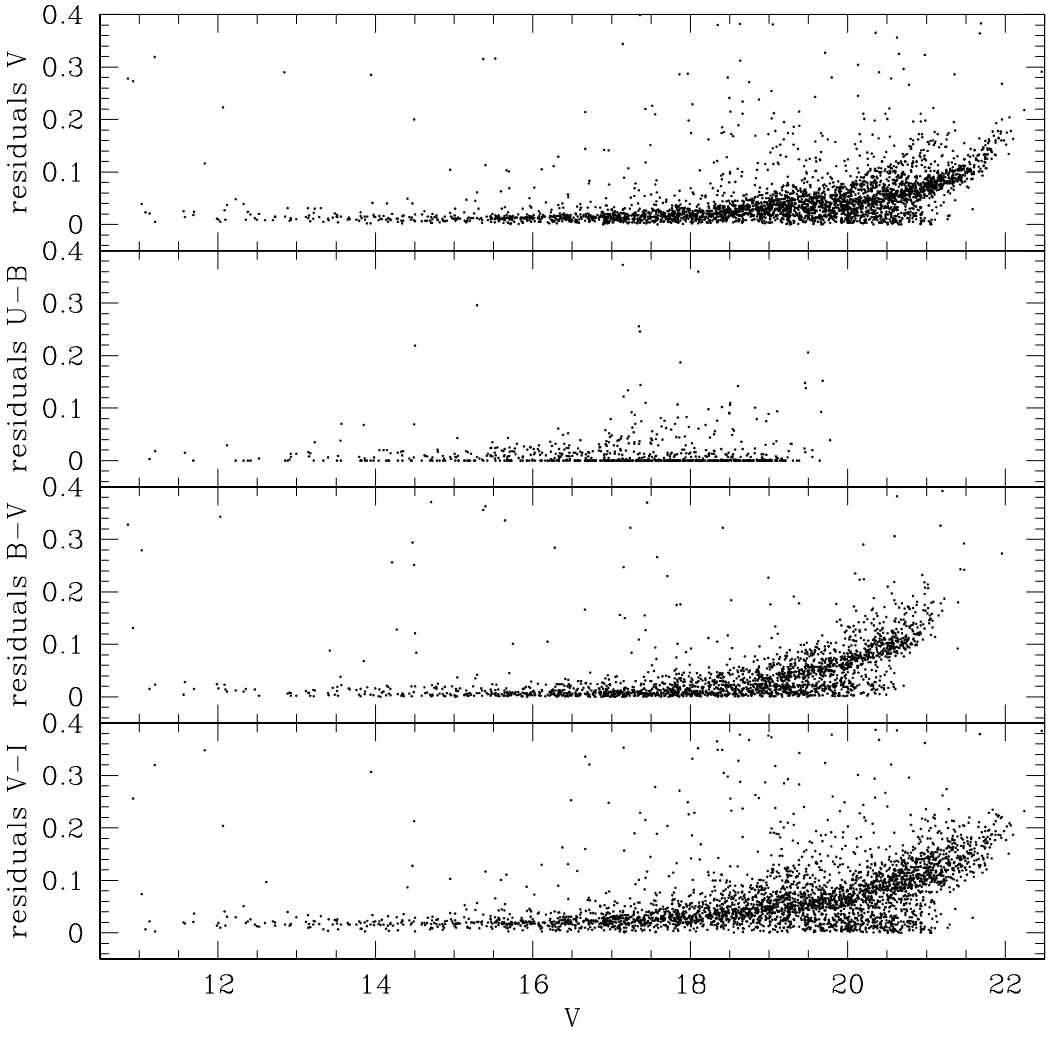

Figure 2. Magnitude and colour photometric errors as a function of V for all the measured stars in the field of NGC 2432. This behaviour is similar for the remaining three clusters.

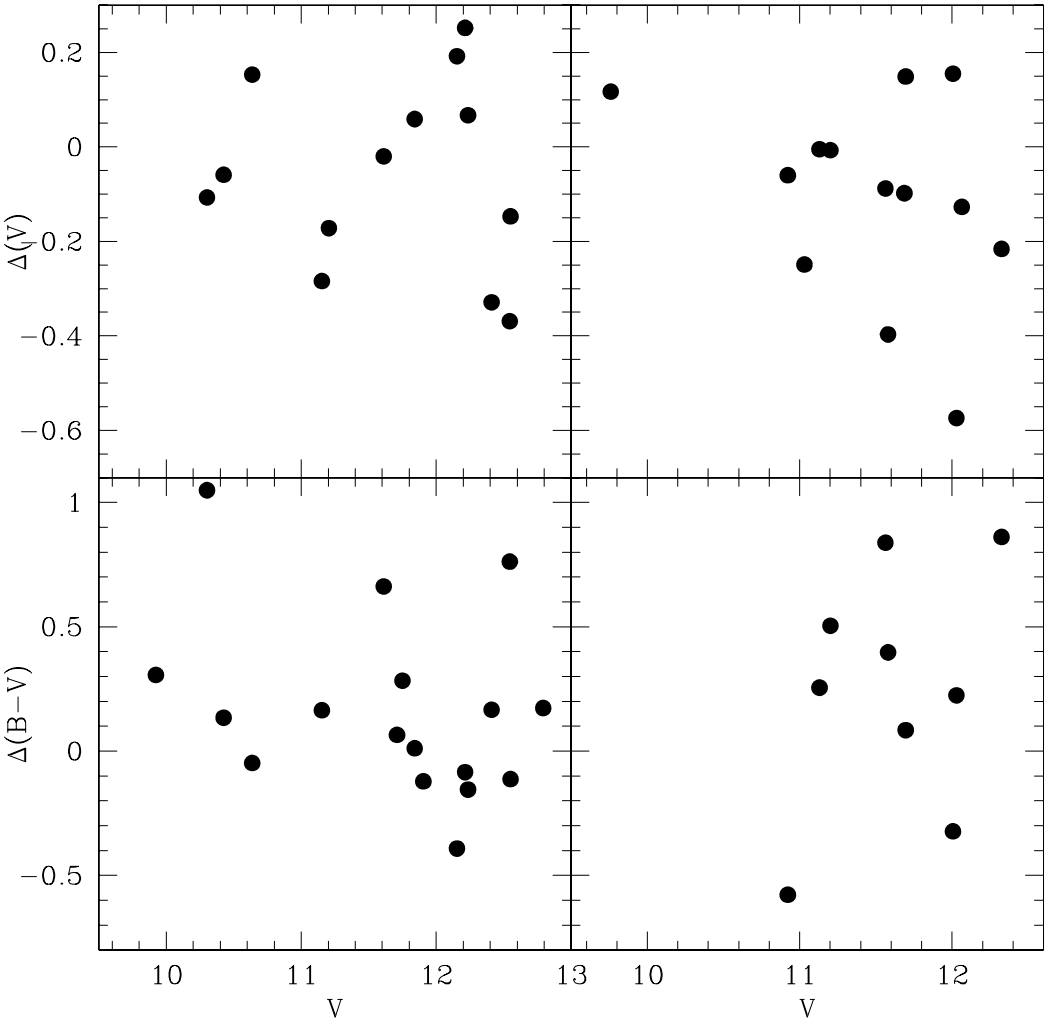

Figure 3. Comparison of our photometry with that of Kharchenko et al. (2005) for (left-hand panels) NGC 2311 and (right-hand panels) NGC 2432.

In particular, stars in the selected area PG 0231+051 were observed at low and high airmasses to adjust the extinction coefficients properly. By the end of each night, we had collected an average of 45 different measures of magnitude per filter for the selected standard star sample.

Table 2 shows the logbook of the observations with filters, exposure times, airmasses and seeing estimates. Observational set-ups, data reduction procedures, stellar point spread function photometry and transformation to the standard system follow the same prescriptions described in detail in Piatti, Clariá & Ahumada (2009). We used linear terms to fit the dependence of the instrumental magnitudes with the effective airmass and the respective colour. Table 3 lists the resulting coefficients for each night, where a, b and c, respectively, represent the zero-point, the airmass coefficient and the colour coefficient. The last two columns list the colour used in the transformation equations and the rms errors revealing that the nights were photometric. Note that we performed two independent V transformations – one with $B - V$ and another with $V - I$ – in order to include stars observed only in the B or I images.

Once the standard magnitudes and colours were obtained by applying the transformation coefficients of Table 3, we produced a master table containing the average of V, $U - B$, $B - V$ and $V - I$, their rms errors $\sigma(V)$, $\sigma(U - B)$, $\sigma(B - V)$ and $\sigma(V - I)$ and the number of observations for each star. For stars with one measure we adopted the photometric errors provided by DAOPHOT.[1] Tables 4–7 provide this information for NGC 2311, Trumpler 6, NGC 2432 and BH 54, respectively. Only a portion of these tables is shown here for guidance regarding their form and content. Tables 4–7 are available in their entirety in the online version of the journal (see Supporting Information). The deepest CCD images obtained for the cluster sample are shown in Fig. 1. The cluster regions are encompassed by the solid circles.

Tables 4–7 show that those stars with three measures of $U - B$, $B - V$ or $V - I$ colours extend from the brightest limit down to $V = 18$, 19 and 20 mag, respectively. The stars with two measures in any of these three colours cover V ranges from 16.0–19.5, 17.0–20.0 and 18.0–21 mag, respectively. Finally, the stars with only one measure of $U - B$, $B - V$ or $V - I$ are fainter than $V = 18.0$, 19.0 and 20.0 mag, respectively, reaching in each case the photometric magnitude limits. Bearing in mind these V ranges for stars with different numbers of observations per filter, we conclude that the stars lying within the ∼6 brightest out of the ∼9 mag range along which our photometry extends were observed either two or three

[1] Programme kindly provided by P. B. Stetson.

times. Therefore, they are more appropriate to derive the cluster fundamental parameters than those observed only once in each filter. The behaviour of the photometric errors for the V magnitude and $U-B$, $B-V$ and $V-I$ colours as a function of V is illustrated in Fig. 2, wherein we have used all the stars measured only in NGC 2432. The behaviour of the photometric errors in the three remaining cluster fields is similar. These errors allow us to rely on the accuracy of the morphology and position of the main cluster features in the CMDs and the colour–colour diagrams.

Using the ASCC-2.5 (Kharchenko 2001), Kharchenko et al. (2005) identified the OCs NGC 2311 and NGC 2432 and applied an iterative procedure to evaluate cluster membership and to determine their basic astrophysical parameters. They reported *BV* photometry for 22 and 30 stars in the fields of NGC 2311 and NGC 2432, respectively, the limiting magnitude being $V \sim 12.5$ mag. Fig. 3 shows a comparison between our photometry and theirs for a handful of stars measured in both clusters. The differences $\Delta V = V_{\rm ketal05} - V_{\rm our}$ and $\Delta(B-V) = (B-V)_{\rm ketal05} - (B-V)_{\rm our}$ as a function of our V magnitudes exhibit noticeable offsets and high dispersions. This result prevents us from trusting the accuracy of the ASCC-2.5 photometry, particularly for bright stars whose images could be saturated. Notice that the errors of our photometry for stars in Fig. 3 are, at most, in the order of the sizes of the plotted symbols. We refer the reader to Section 6 where a detailed analysis of Kharchenko et al.'s (2005) results is dealt with.

3 COLOUR–MAGNITUDE AND COLOUR–COLOUR DIAGRAMS ANALYSIS

3.1 Colour–magnitude diagrams cleaning

The resulting CMDs and colour–colour diagrams are drawn in Figs 4–7 which show broad star sequences. Unless a thorough analysis of such sequences is made, one might conclude that they are in fact the clusters' main sequences (MSs). However, all the CMDs and colour–colour diagrams reveal both cluster and field star MSs more or less superimposed. Thus, in order to estimate the cluster fundamental parameters from their CMDs and colour–colour diagrams, we should first be able to separate the cluster MSs stars from those belonging to the surrounding fields. Note that both cluster and field stars are, in general, affected by nearly the same interstellar reddening, which is indeed what causes the overlapping of their

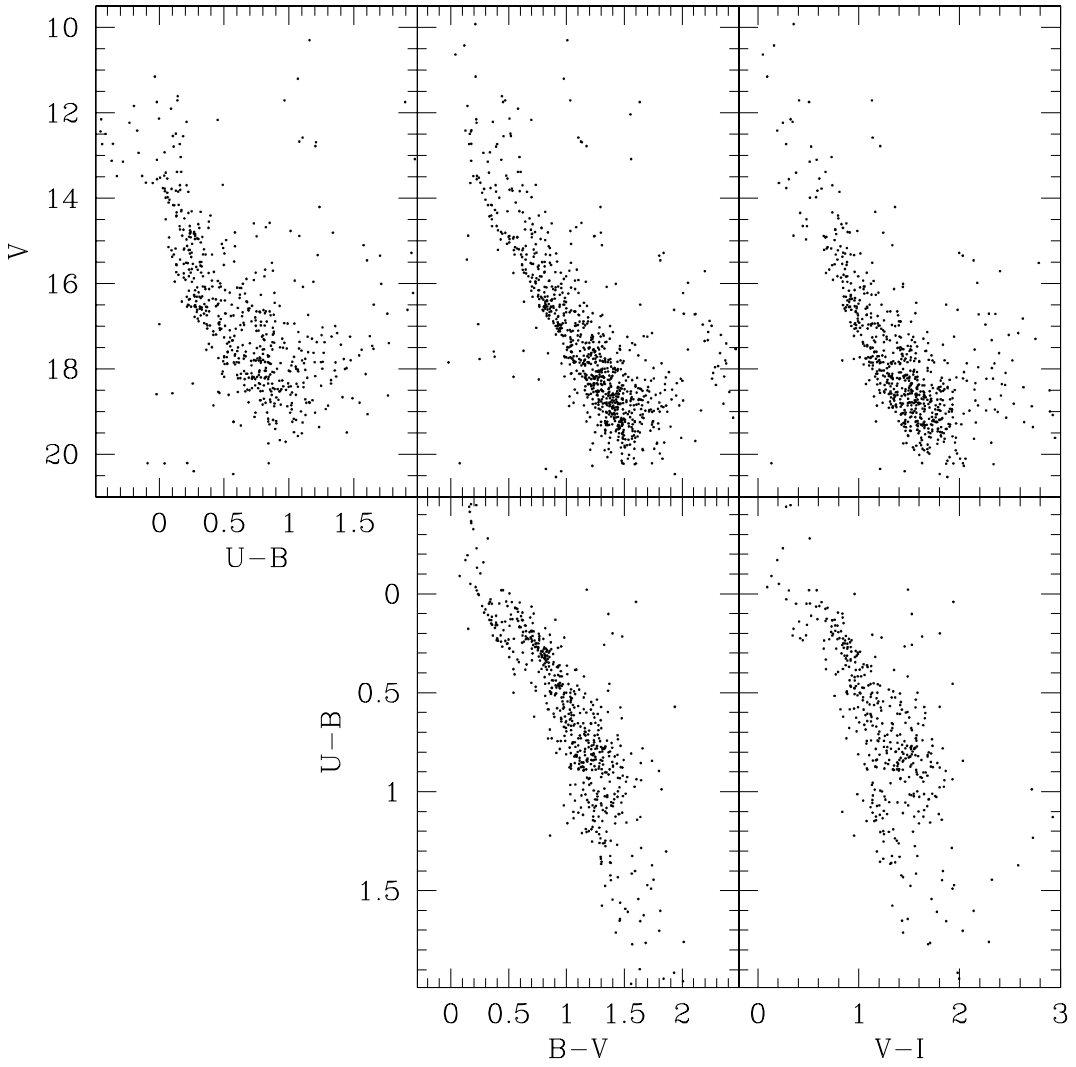

Figure 4. Top: $(V, U-B)$, $(V, B-V)$ and $(V, V-I)$ diagrams; and bottom: $(U-B, B-V)$ and $(B-V, V-I)$ diagrams, for the stars measured in the field of NGC 2311.

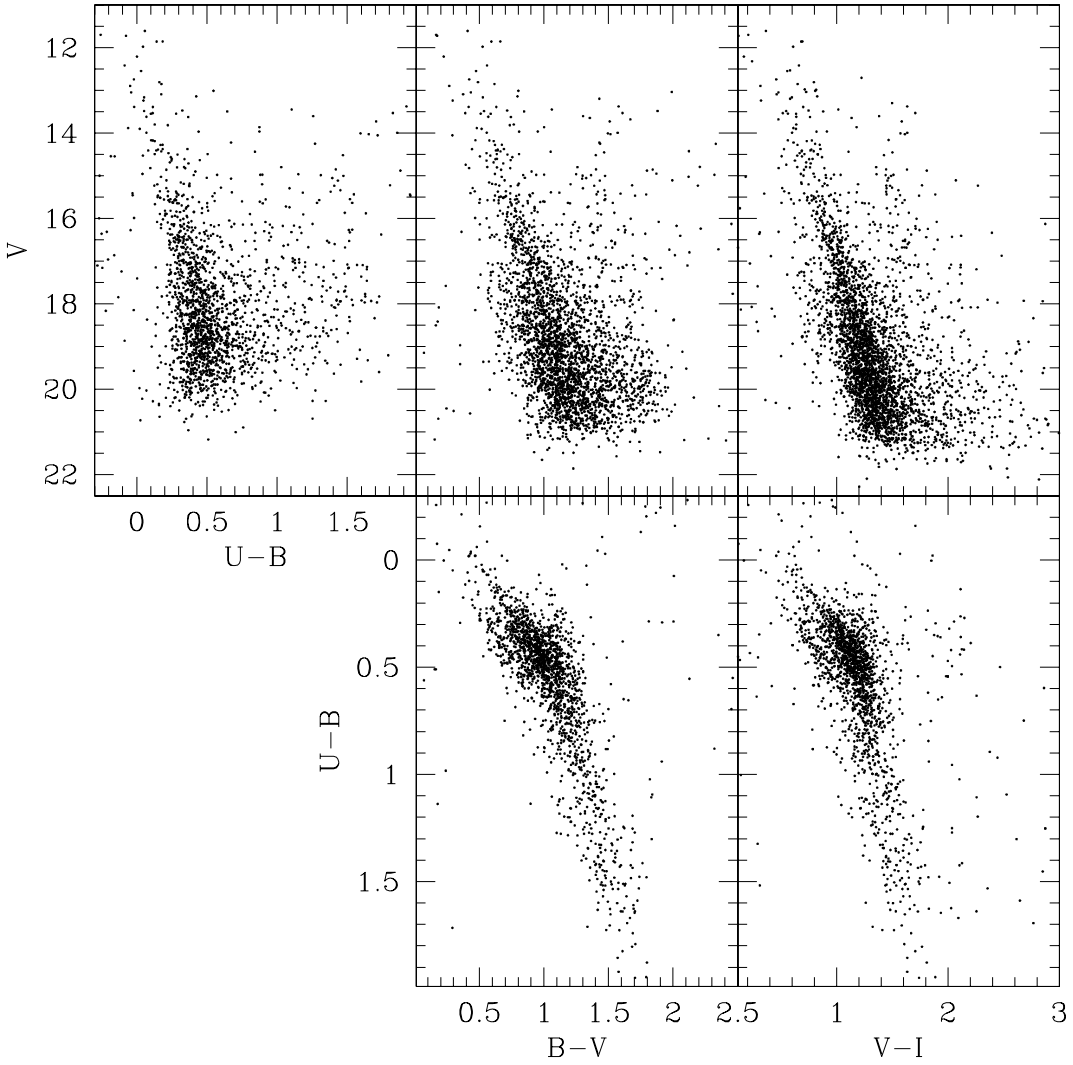

Figure 5. Top: $(V, U-B)$, $(V, B-V)$ and $(V, V-I)$ diagrams; and bottom: $(U-B, B-V)$ and $(B-V, V-I)$ diagrams, for the stars measured in the field of Trumpler 6.

MSs. This fact makes the cleaning of the CMDs and colour–colour diagrams even more difficult.

To filter the field stars from the CMDs and colour–colour diagrams, we applied a statistical procedure. Such method consists in adopting the CMDs built using the stars located in the easternmost strip of the observed fields, i.e. $x < 500$ pixels and $0 < y$ (pixels) < 2050 (see Fig. 1), as reference to statistically filter the remaining observed areas ($x > 500$ pixels and $0 < y$ (pixels) < 2050) in each cluster. Using these field CMDs, we counted how many stars lie in different magnitude–colour bins with sizes $[\Delta V, \Delta(U-B) = \Delta(B-V) = \Delta(V-I)] = (0.5, 0.2)$ mag. We then subtracted from the $x > 500$ pixels CMDs the number of stars counted for each bin of the field [V, ($U-B$, $B-V$ or $V-I$)] CMDs, by removing those stars closer in magnitude and colour to the ones in the star fields. With the aim of comparing the resulting residuals, we carried out this filtering procedure by using bins of (1.0, 0.2) and (0.5, 0.1) mag. The application of this method rendered four additional tables similar to Tables 4–7, one per observed cluster field. Each of them contains the stars located within the region delimited by $x > 500$ pixels and $0 < y$ (pixels) < 2050 that have not been subtracted once we eliminated those matching the spatial density, magnitude and colour distributions of the easternmost strip of the observed fields.

3.2 Cluster dimensions and structures

We used the resulting tables of Section 3.1 to determine the location of the clusters' centres in order to construct the clusters' stellar density profiles. The coordinates of the geometrical clusters' centres and their estimated uncertainties were determined by fitting Gaussian distributions to the star counts in the x and y directions. The fits of the Gaussians were performed using the NGAUSSFIT routine in the STSDAS/IRAF[2] package. We adopted a single Gaussian and fixed the constant and the linear terms to zero. The stars projected along the x and y directions were counted within intervals of 50 pixels wide. In addition, we checked that the use of spatial bins from 20 to 50 pixels

[2] IRAF is distributed by the National Optical Astronomy Observatories, which is operated by the Association of Universities for Research in Astronomy, Inc., under contract with the National Science Foundation.

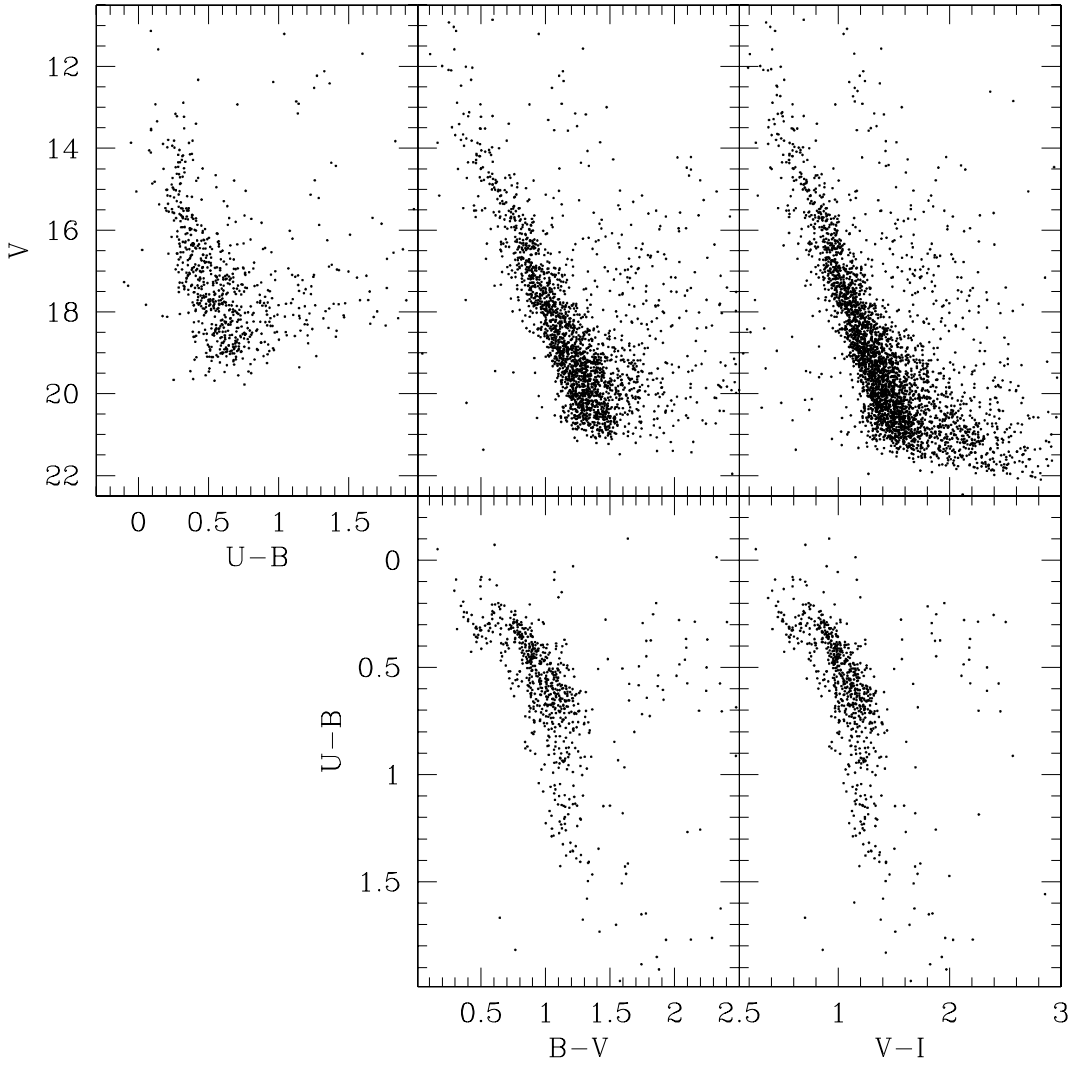

Figure 6. Top: $(V, U-B)$, $(V, B-V)$ and $(V, V-I)$ diagrams; and bottom: $(U-B, B-V)$ and $(B-V, V-I)$ diagrams, for the stars measured in the field of NGC 2432.

or from 50 to 100 pixels does not lead to significant changes in determining the centres. We iterated the fitting procedure once on average, after eliminating a couple of discrepant points. Then, we determined the clusters' centres with a typical NGAUSSFIT standard deviation of ±30 pixels.

We also fixed the clusters' centres by making use of the N2GAUSSFIT program in the STSDAS/IRAF package, which allows a two-dimensional elliptical Gaussian fit represented by the Gaussian amplitude, the x and y centres, the full width at half-maximums (FWHMs), the ellipticity, the position angle and the background level. We selected the deepest V images of the clusters and kept all seven coefficients so that they could be modified during the fit. After a few iterations varying the size of the windows which defined the fitted areas, we derived the best values of the seven coefficients based on the smallest obtained χ^2 and rms values and individual coefficient errors. Finally, we averaged the clusters' centres determined by NGAUSSFIT, N2GAUSSFIT and by the visual inspection of the observed NGC 2311, Trumpler 6, NGC 2432 and BH 54 fields. The resulting (x_c, y_c) values are (1430, 1340), (1080, 970), (1220, 1240) and (1270, 950) pixels, respectively.

We then constructed the clusters' radial profiles based on star counts within boxes of 50 pixels a side distributed throughout the whole cleaned field of each cluster. The chosen size of the box allowed us to statistically sample the star spatial distributions and to avoid spurious effects caused mainly by the presence of localized groups, rows or columns of stars. Therefore, the number of stars per unit area at a given radius r can be directly calculated through the expression

$$(n_{r+25} - n_{r-25}) / \left((m_{r+25} - m_{r-25})\, 50^2 \right), \quad (1)$$

where n_j and m_j represent the number of stars and boxes included in a circle of radius j, respectively. Note that this method does not necessarily require a complete circle of radius r within the observed field to estimate the mean stellar density at such distance. This is an important consideration since having a stellar density profile which extends far away from the cluster centre allows us to trace the cluster outer regions with higher precision. The resulting density profiles are shown in Fig. 8, where the error bars at various distances from the cluster centres follow Poisson statistics. From this figure we adopted angular radii of 600, 400, 500 and 250 pixels, equivalent to 4.0, 2.7, 3.3 and 1.7 arcmin, for NGC 2311, Trumpler 6, NGC 2432 and BH 54, respectively. Uncertainties are estimated between 100 and 150 pixels. Therefore, the four studied OCs turned out to be somewhat smaller than previously believed. To illustrate the

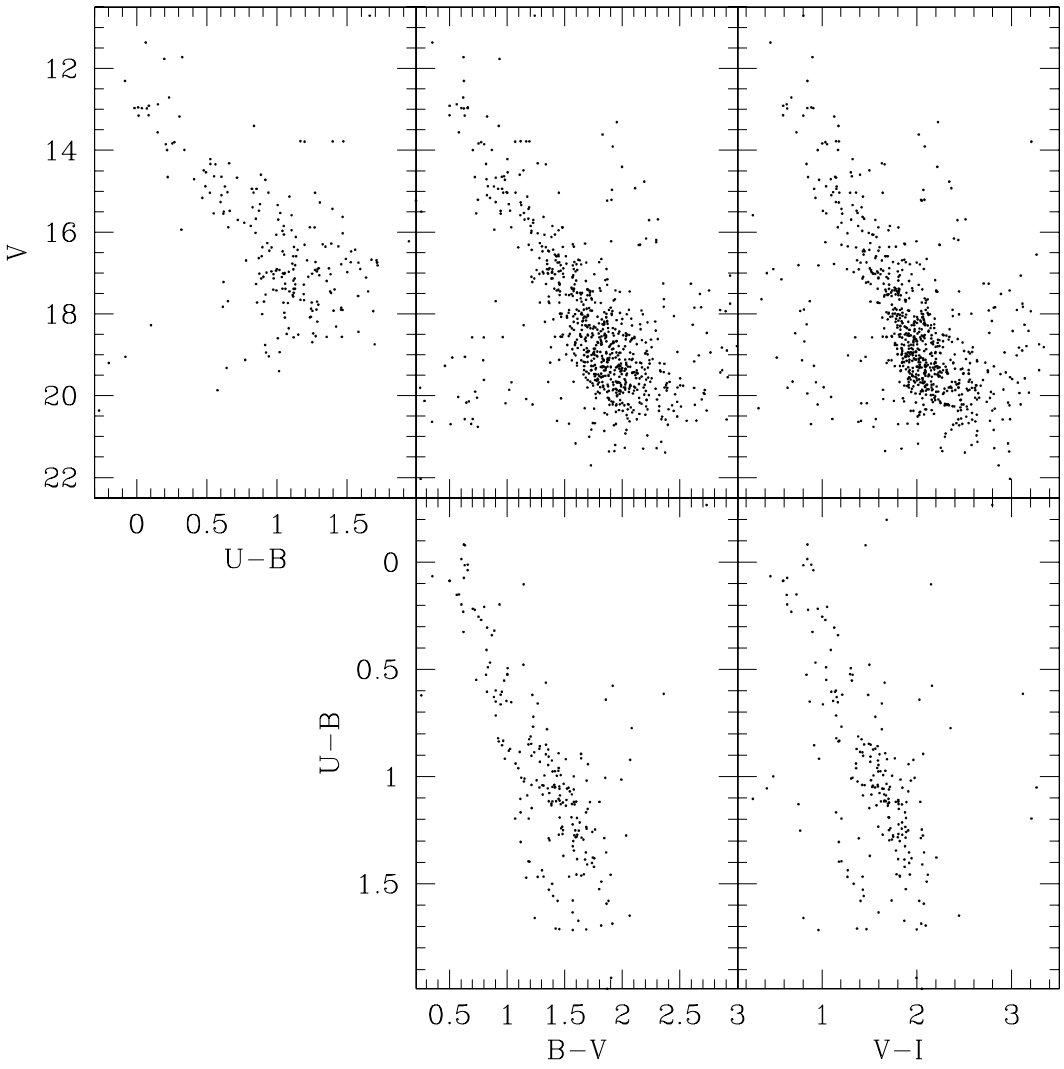

Figure 7. Top: $(V, U-B)$, $(V, B-V)$ and $(V, V-I)$ diagrams; and bottom: $(U-B, B-V)$ and $(B-V, V-I)$ diagrams, for the stars measured in the field of BH 54.

encompassed regions where the clusters mainly extend, we plotted representative circles in Fig. 1.

4 CLUSTER COLOUR–MAGNITUDE DIAGRAMS: MEMBERSHIP CRITERIA

Using CMDs and colour–colour diagrams cleaned from field star contamination obtained in Section 3.1 and the circles for the cluster regions adopted in Section 3.2, we applied the criteria defined by Clariá & lapasset (1986) to evaluate the membership status of the measured stars. First, it is required that the location of a star in the two colour–colour diagrams is close to the MS of the cluster, the maximum accepted separation being 0.10 mag. The second requirement is that the location of the same star in the three CMDs corresponds to the same evolutionary stage.

To identify which stars fulfil the criteria stated above, we superimposed the zero-age main-sequence (ZAMS) of Lejeune & Schaerer (2001) to the observed $(U-B, B-V)$ diagram by adopting a colour excess $E(B-V) = E_o$, which corresponds to the bluest envelope of the observed sequence. Then, we looked for every star closer than 0.10 mag from the ZAMS. The location of the ZAMS in this $(U-B, B-V)$ diagram also requires the knowledge of the slope value for the reddening line. Although it is well known that there are variations in the reddening law throughout the Galaxy (Turner 1994), a mean reddening slope of $E(U-B)/E/B-V) = 0.72$ is usually found for most Galactic longitudes. If we adopt $E(V-I)/E(B-V) = 1.25$ (Dean, Warren & Cousins 1978), this value implies the following ratio: $E(U-B)/E(V-I) = 0.72/1.25 = 0.58$. Thus, by sliding the ZAMS according to this reddening line in the $(U-B, V-I)$ diagram, we discarded as cluster members all stars that fall beyond 0.10 mag from the ZAMS. Next, using all the stars that complied with this first requirement, we kept as probable members those stars whose locations correspond to the same evolutionary stage in the three CMDs. With that in mind, we superimposed the ZAMS to the three CMDs and adopted the above $E(B-V)$ value using the apparent distance modulus $V - M_V$ which best fits the ZAMS to the unevolved star sequence. Finally, by carefully inspecting the three CMDs and the two colour–colour diagrams, we could distinguish the possible cluster members. We repeated this procedure for different $E(B-V)$ values increasing them in steps of 0.05 mag each time, until reaching the reddest envelope of the observed sequence. Finally, we adopted the $E(B-V)$ value for which we obtained the

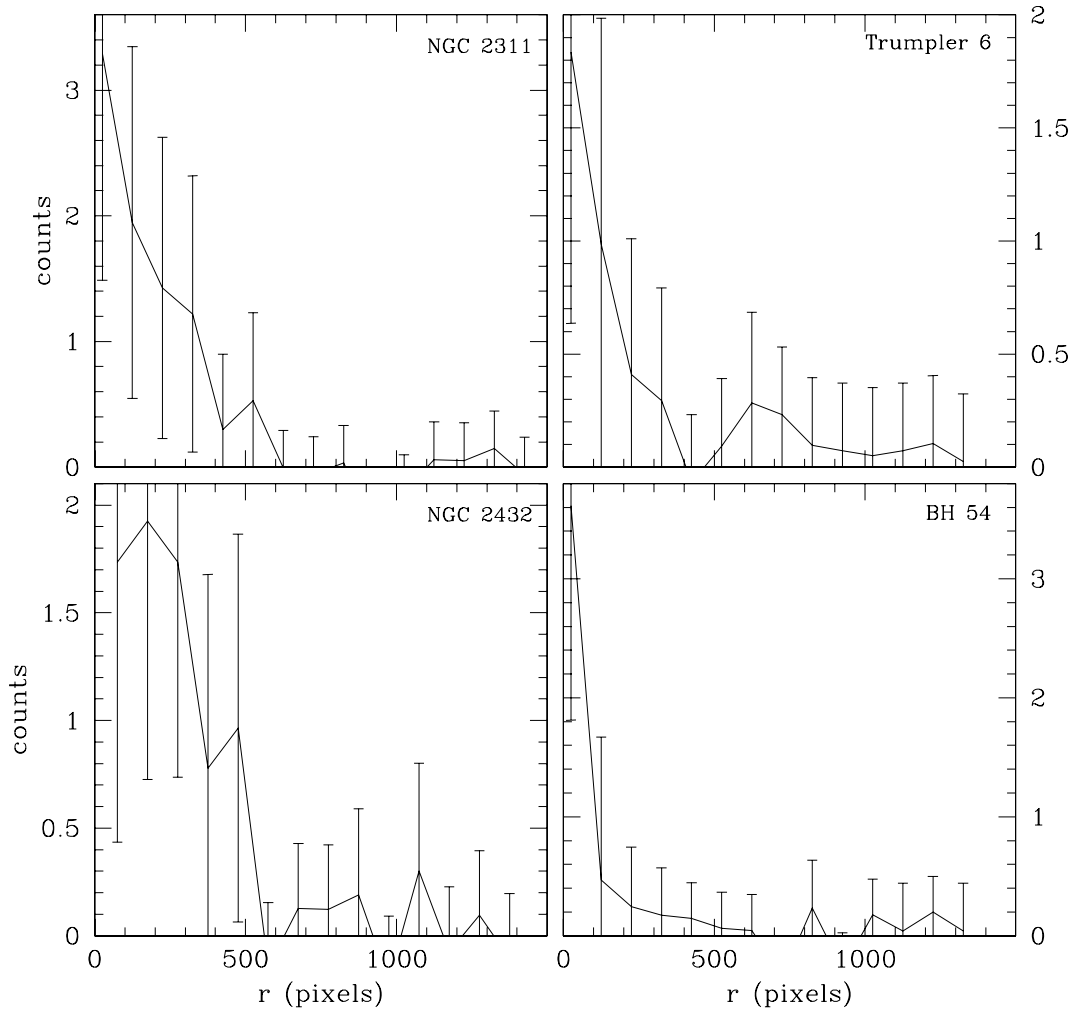

Figure 8. Stellar density profiles for the studied clusters. Error bars at various distances from the cluster centres follow Poisson statistics.

most populous MS. We recall that no star sequence survives for $E(B-V)$ values different from those corresponding to the cluster MSs.

We show in Figs 9–12 the CMDs and colour–colour diagrams directly obtained with all the measured stars located within the circular regions of Fig. 1 (dots). In the same figures, we also overplotted the cleaned diagrams obtained in Section 3.1 (open circles), as well as the probable cluster members according to the above photometric criteria (filled circles). The ZAMSs, appropriately shifted by the cluster colour excesses and distance moduli, were also superimposed. When comparing the cleaned and fiducial cluster CMDs and colour–colour diagrams observed, the differences in stellar composition became evident. Although the fiducial features of the OCs looked clearer, some unavoidable field interlopers could also be present. Photometric errors, evolutionary and/or binarity effects can also be responsible for the dispersion in their CMDs.

4.1 Interstellar extinction

The method described assumes that the colour excesses are uniform across the observed fields. Nevertheless, sometimes the colour excesses in certain regions of the sky are not uniform at all. We used the reddening maps of Schlegel, Finkbeiner & Davis (1998, hereafter SFD) to corroborate our assumption. SFD obtained full-sky maps from 100-μm dust emission. They found that in high Galactic latitude regions, the dust map correlates well with maps of H I emission. However, deviations are coherent in the sky and are especially conspicuous in regions of H I emission saturation toward denser clouds and in regions of formation of H_2 in molecular clouds (Piatti et al. 2003, 2008). Even if the SFD's reddenings were not totally correct due to the low Galactic latitudes of the studied OCs, it may still be useful to consider their values for the observed fields. We computed $E(B-V)_{\rm SFD}$ colour excesses for grids in the (l, b) Galactic coordinate plane, with steps of $\Delta(l, b) = (0.^\circ01, 0.^\circ01)$, thus covering the whole observed fields of Fig. 1. Then, for the resulting $E(B-V)_{\rm SFD}$ values, we built the histograms shown in Fig. 13, where we included at the top of each panel the $E(B-V)$ colour excesses estimated from our previous analysis. Since the mean $E(B-V)$ values turned out to be considerably larger than any value expected from the observed $(U-B, B-V)$ diagrams, we assumed that the $E(B-V)_{\rm SFD}$ values must be saturated. However, it is worth considering that the 1σ dispersion of the different histograms is smaller than 0.11 (except for the possible marginal case of BH 54), the lowest limit estimated by Burki & Maeder (1973) for clusters with differential reddening. So we believe that the

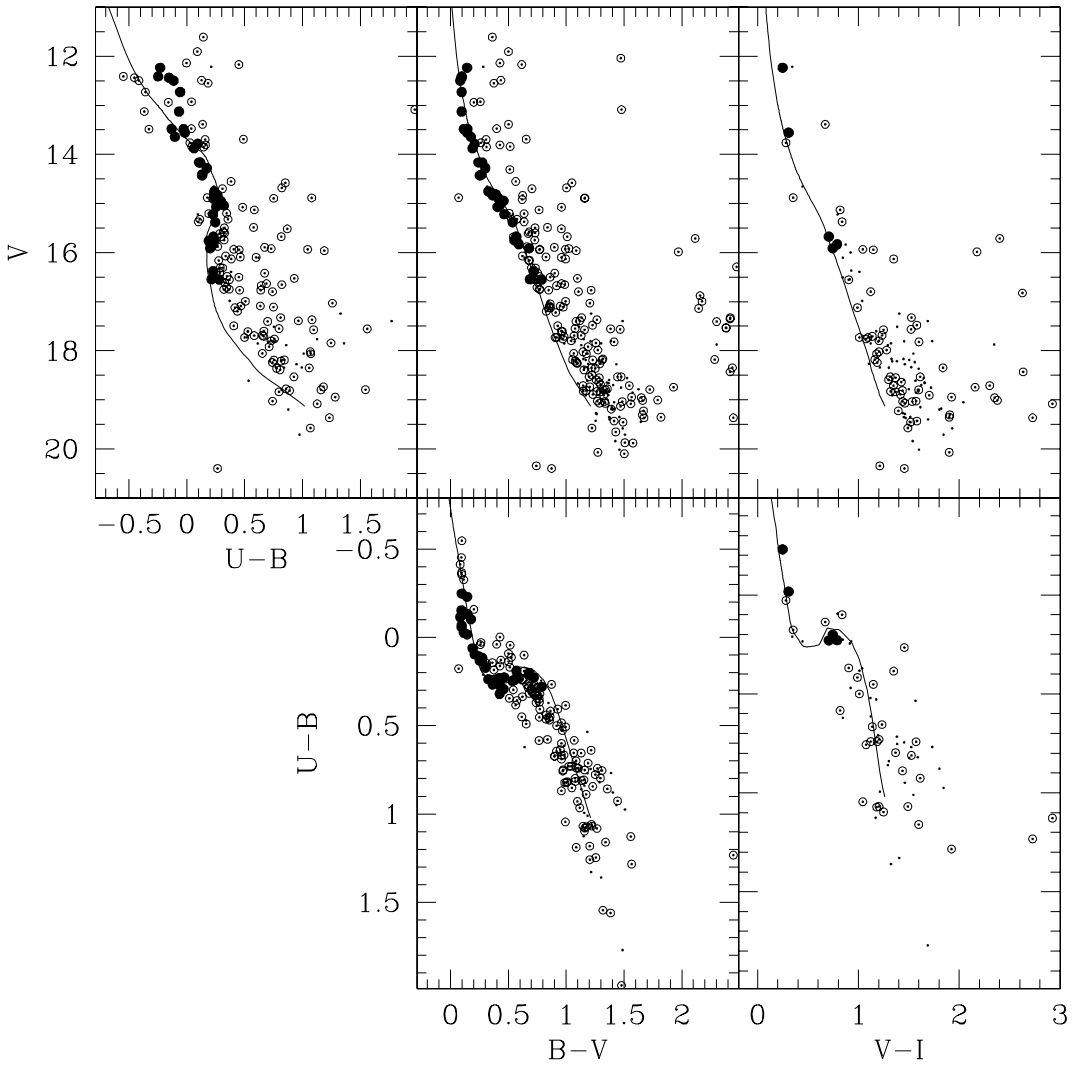

Figure 9. Top: extracted (V, $U-B$), (V, $B-V$) and (V, $V-I$) diagrams; and bottom: ($U-B$, $B-V$) and ($U-B$, $V-I$) diagrams, for NGC 2311. Dots, open circles and filled circles represent the observed, cleaned and cluster diagrams, respectively. The ZAMS for luminosity class V stars is overplotted.

interstellar reddening across the observed fields can be considered uniform within the quoted uncertainties.

5 ESTIMATES OF THE CLUSTERS' FUNDAMENTAL PARAMETERS

We used the derived reddenings, the apparent distance moduli (Section 4) and the most frequently used values for the $A_V/E(B-V)$ ratio (=3.2; Straizys 1992) to obtain the cluster true distance moduli ($V_o - M_V$), the heliocentric distances (d) and the linear radii (r). The distance errors were computed with the expression $\sigma(d) = 0.46[\sigma(V-M_V) + 3.2\sigma\ (E(B-V))]d$, where $\sigma(V-M_V)$ and $\sigma(E(B-V))$ represent the estimated errors in $V-M_V$ and $E(B-V)$, respectively. By using the cluster Galactic coordinates (l, b) and the calculated heliocentric distances, we derived the cluster (X, Y, Z) coordinates and their Galactocentric distances, assuming the Sun's distance from the centre of the Galaxy to be 8.5 kpc. The resulting cluster parameter values are presented in Table 8.

The widely used procedure of fitting theoretical isochrones to the observed CMDs was employed to estimate the cluster ages. We fitted isochrones computed by Lejeune & Schaerer (2001) to the cluster (V, $U-B$), (V, $B-V$) and (V, $V-I$) CMDs. The isochrones which cover an age range from 10^3 yr to 16–20 Gyr, in steps of $\Delta\log t = 0.05$ dex, were calculated for the entire set of non-rotating Geneva stellar evolution models. These isochrones cover star masses from 0.4–0.8 to 120–150 $M_\odot$ and star metallicities from $Z = 0.0004$ to 0.1. When we selected subsets of isochrones for different Z values to assess the metallicity effect in the cluster fundamental parameters, we preferred to choose those including overshooting effect. We followed the general rule of adopting a chemical composition of $Z = 0.020$ (solar metallicity) for the isochrone sets. This is a representative metallicity for most of the OCs studied in detail located between 1 and 2 kpc from the Sun (Mermilliod & Paunzen 2003).

Next, we selected a large number of isochrones and used the derived pair of distance modulus and reddening values to estimate the cluster ages. The brightest magnitude in the MS and the bluest point of the turn-off were used as reference points when the fits were being made. The reddening and distance modulus uncertainties were estimated bearing in mind the dispersion of the cluster MSs and the mentioned reference points. Table 8 lists the possible solutions for the cluster ages that prove to be consistent with the data obtained,

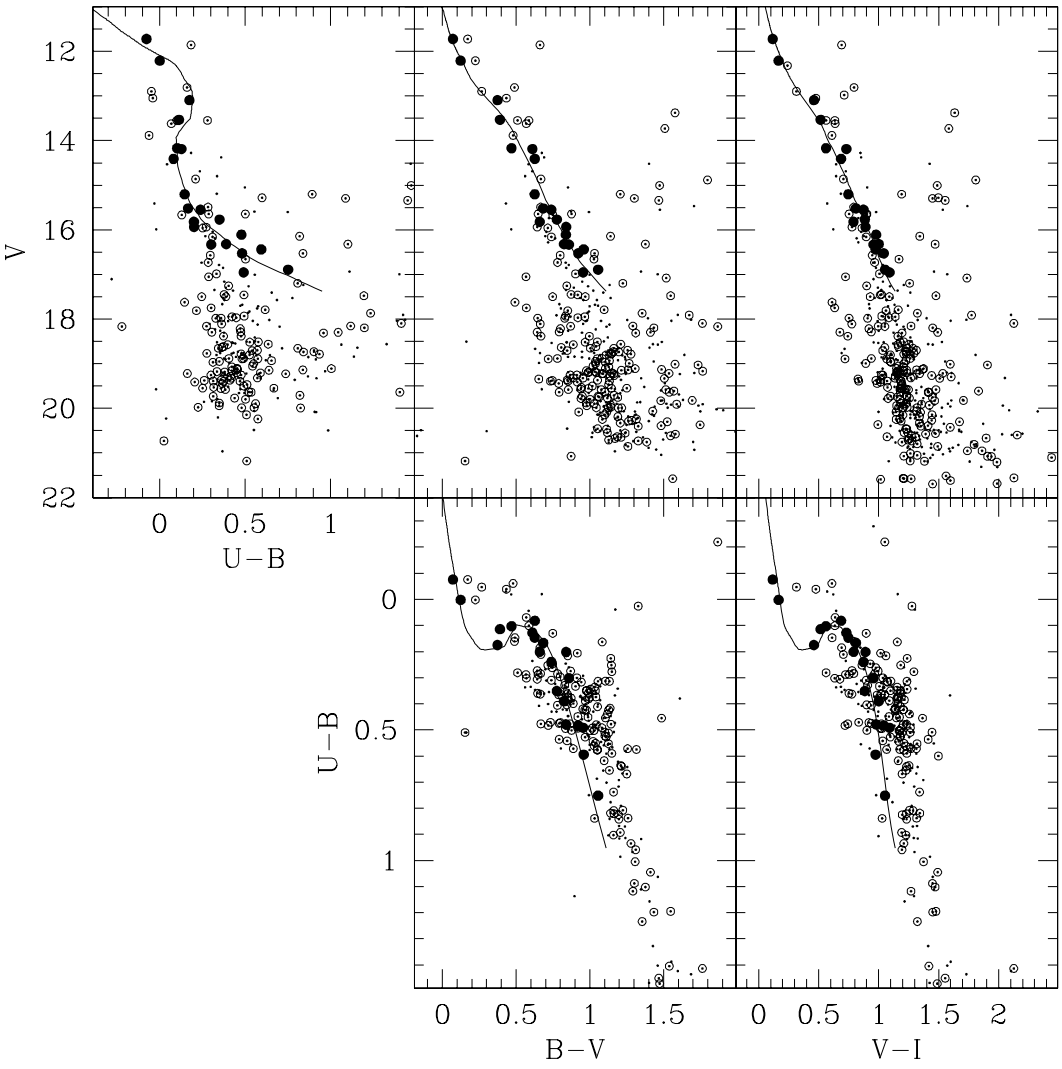

Figure 10. Top: extracted (V, $U-B$), (V, $B-V$) and (V, $V-I$) diagrams; and bottom: ($U-B$, $B-V$) and ($U-B$, $V-I$) diagrams, for Trumpler 6. Dots, open circles and filled circles represent the observed, cleaned and cluster diagrams, respectively. The ZAMS for luminosity class V stars is overplotted.

in the sense that they most accurately reproduce the cluster features in the three CMDs. Figs 14–17 illustrate how the isochrones used match the cluster features in the CMDs. For comparison purposes, we included as dotted lines in the mentioned figures the isochrones associated to the cluster age errors.

5.1 2MASS photometry

Although the four clusters have been studied here only in the optical spectral range, the availability of the Two Micron All-Sky Survey (2MASS)[3] photometric catalogue (Skrutskie et al. 2006) becomes a very valuable tool for different reasons. On the one hand, if a properly shifted isochrone satisfactorily matches the (V, $B-V$) CMD and the 2MASS (J, $J-H$) one for a cluster, this means that both independent photometric scales are consistent. On the other hand, a successful isochrone matching in the near-infrared region using stars adopted as cluster members from the *UBVI* analysis reinforces our belief that the cluster members have been correctly identified. Thus, we extracted near-infrared J, H and K_s 2MASS photometry for all the probable photometric members in the four studied OCs and built the corresponding (J, $J-H$) and (J, $J-K_s$) CMDs. A typical distribution of the photometric uncertainties as a function of magnitude can be found in Bonatto & Bica (2007). About 75–85 per cent of the stars have errors in the J, H and K_s magnitudes smaller than 0.06 mag.

Using the ages, apparent distance moduli and reddenings derived for the cluster sample, we superimposed the theoretical isochrones computed by Lejeune & Schaerer (2001) on to the cluster (J, $J-H$) and (J, $J-K_s$) CMDs, once they were shifted by the corresponding $J-M_J$, $E(J-H)$ and $E(J-K_s)$ values. We converted $E(B-V)$ to $E(J-H)$ and $E(J-K_s)$ and $V-M_V$ to $J-M_J$ using the relations $A_J/A_V = 0.276$, $A_H/A_V = 0.176$, $A_{K_s}/A_V = 0.118$, $A_J = 2.76E(J-H)$ and $E(J-H) = 0.33E(B-V)$ (Dutra, Santiago & Bica 2002). The results of this task are illustrated in Fig. 18, which confirms the consistency between the 2MASS photometric scale and ours as well as our previous photometric membership assessment of the cluster stars.

[3] The 2MASS available at http://irsa.ipac.caltech.edu/

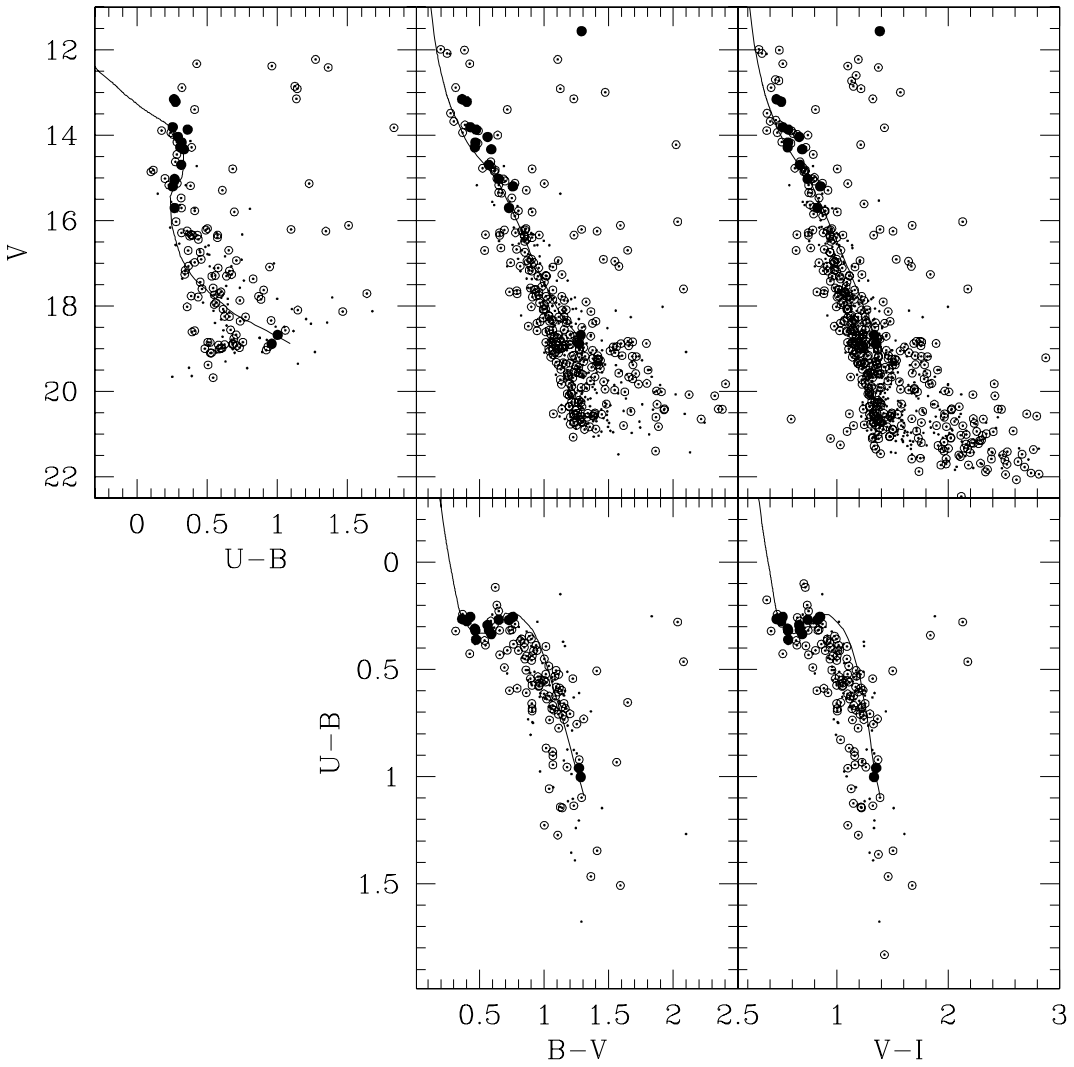

Figure 11. Top: extracted (V, $U-B$), (V, $B-V$) and (V, $V-I$) diagrams; and bottom: ($U-B$, $B-V$) and ($U-B$, $V-I$) diagrams, for NGC 2432. Dots, open circles and filled circles represent the observed, cleaned and cluster diagrams, respectively. The ZAMS for luminosity class V stars is overplotted.

6 COMPARISON WITH EARLIER RESULTS

Based on the ASSC-2.5 (Kharchenko 2001), Kharchenko et al. (2005) gathered proper motions in the *Hipparcos* system and B, V magnitudes in the Johnson photometric system for 22 and 30 stars in the fields of NGC 2311 and NGC 2432, respectively. They also supplemented these data with spectral types and radial velocities. On the one hand, they applied an iterative procedure for cluster membership determination based on proper motions and photometric and spatial criteria. On the other hand, they estimated the mean cluster proper motions and radial velocities as well as the reddenings, distances and ages for both clusters. Figs 19 and 20 (upper left-hand panels) show the relation between the membership probabilities coming from proper motions ($P_{\rm pm}$) and the (V, $B-V$) CMDs ($P_{\rm CMD}$) for NGC 2311 and NGC 2432, respectively. We have represented with filled, crossed and starred circles stars with $P_{\rm pm}$ and $P_{\rm CMD} > 70$ per cent, with $P_{\rm pm} > 70$ per cent and with $P_{\rm CMD} > 70$ per cent, respectively. Open circles denote stars with a chance lower than 70 per cent of being a probable cluster member according to both independent procedures. As can be seen, three stars in NGC 2311 and five stars in NGC 2432 appear to be firm candidate members (filled circles). However, those stars are distributed outside the circles traced in Fig. 1. For comparison purposes, these schematic finding charts (Figs 19 and 20) have the same coordinate systems as in Fig. 1. Surprisingly, stars with higher membership probabilities (filled circles) do not have V magnitudes and $B-V$ colours consistent with the cluster fundamental parameter solutions found by Kharchenko et al. (2005), since the isochrone for the derived cluster age (NGC 2311 = 400 Myr, NGC 2432 = 150 Myr) shifted by the corresponding colour excesses (NGC 2311 = 0.20 mag, NGC 2432 = 0.12 mag) and apparent distance moduli (NGC 2311 = 12.13 mag, NGC 2432 = 11.91 mag) do not match the (V, $B-V$) CMDs properly (see lower right-hand panel of Figs 19 and 20, respectively).

According to our photometric data and analysis (see Sections 3 and 4), the probable cluster members 8 and 11 in NGC 2311 and 6 and 16 in NGC 2432 (identification numbers from Kharchenko et al. 2005) have known proper motions in the *Hipparcos* system. The mean values and dispersions turned out to be $(\mu_\alpha\cos(\delta), \mu_\delta)_{\rm NGC\,2311} = (1.22 \pm 0.80, -1.52 \pm 4.00)$ mas yr^{-1} and

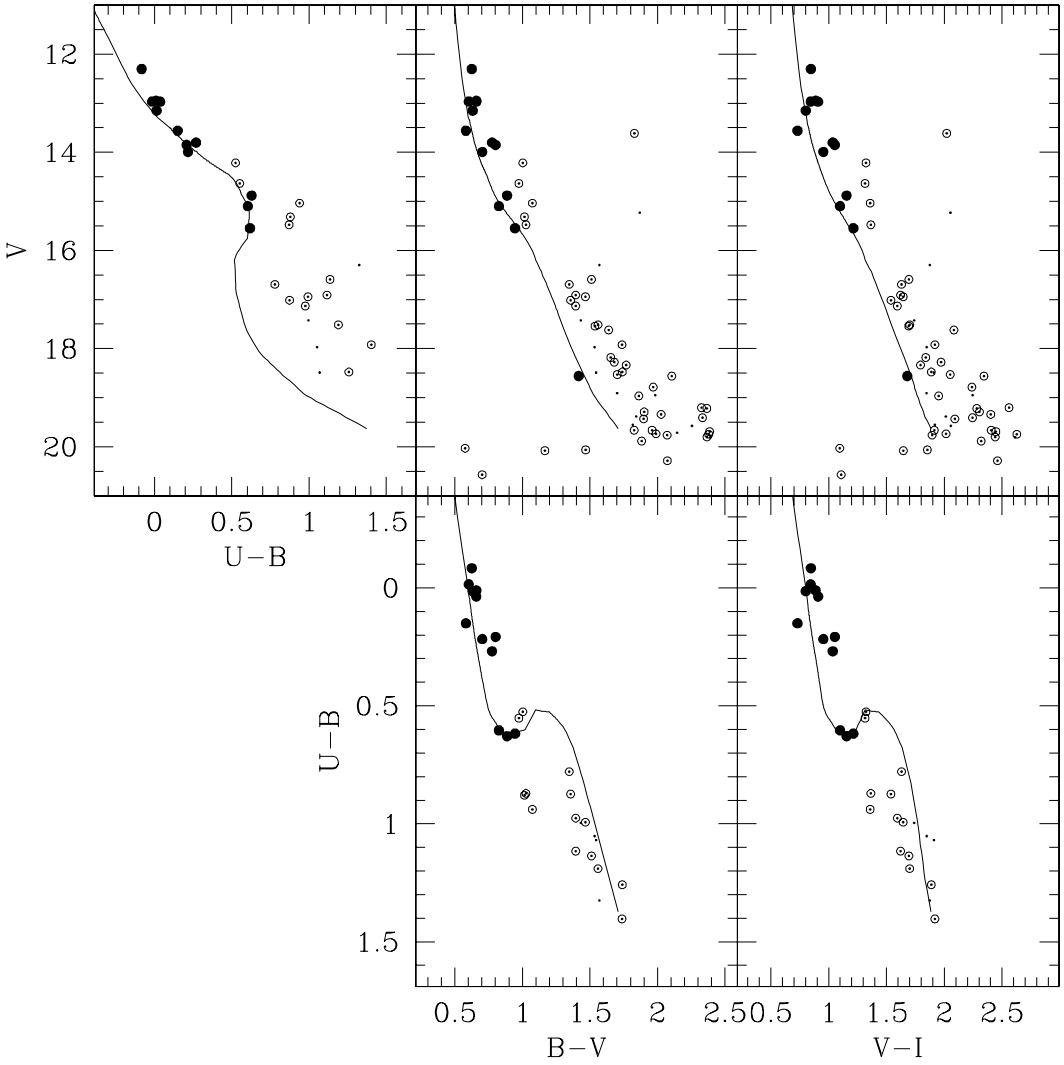

Figure 12. Top: extracted (V, $U-B$), (V, $B-V$) and (V, $V-I$) diagrams; and bottom: ($U-B$, $B-V$) and ($U-B$, $V-I$) diagrams, for BH 54. Dots, open circles and filled circles represent the observed, cleaned and cluster diagrams, respectively. The ZAMS for luminosity class V stars is overplotted.

$(\mu_\alpha\cos(\delta),\ \mu_\delta)_{\rm NGC\,2432} = (-2.89 \pm 2.27,\ 2.53 \pm 0.66)\,{\rm mas\,yr^{-1}}$. In the case of NGC 2311, there is no good agreement with the mean values derived by Kharchenko et al., which are $(\mu_\alpha\cos(\delta),\ \mu_\delta)_{\rm NGC\,2311} = (-3.20,\ +2.77)\,{\rm mas\,yr^{-1}}$ (see also lower left-hand panel of Fig. 19). On the other hand, the mean values for NGC 2432 agree reasonably well with those derived for this cluster by Kharchenko et al. [$(\mu_\alpha\cos(\delta),\ \mu_\delta)_{\rm NGC\,2432} = (-3.68,\ +1.62)\,{\rm mas\,yr^{-1}}$; see also lower left-hand panel of Fig. 20].

Note, however, that the errors for the proper motion measurements quoted by Kharchenko et al. range from 1.5 to 4.5 mas yr^{-1} with an average of 2.7 mas yr^{-1} for stars brighter than $V \approx 12.2$. Hence, no conclusive result can be derived regarding the dynamics of the clusters until more accurate kinematical data for a larger sample of stars are obtained. For instance, it would be desirable to have proper motions available for the present probable cluster members ($V < 16$), which are not included in Kharchenko et al.'s (2005) sample. These proper motions are necessary to obtain a significant statistical sample of both clusters' stars to compare photometric and kinematic membership probabilities. We conclude that NGC 2311 and NGC 2432 are clear examples in the sense that sometimes the proper motions of a single star do not constitute by themselves proof of the cluster membership status of such star. On the other hand, the combined use of both the kinematic (proper motions) and photometric membership probabilities made by Kharchenko et al. (2005) did not seem to reliably estimate the cluster fundamental parameters, either (see Figs 19 and 20).

Ahumada et al. (2007) also determined reddening and age of NGC 2311 from the comparison of the observed integrated cluster spectrum with template spectra of OCs with well known fundamental parameters, as well as from the measurements of the Balmer line equivalent widths. They derived for NGC 2311 an age of about 200–350 Myr and $E(B-V) = 0.15$ from template matching, while the age obtained from the Balmer lines turned out to be within the 200–250 Myr range. However, since the stellar field over which NGC 2311 is projected is certainly very rich, it is quite probable that the cluster-integrated light is strongly contaminated by foreground/background stars. We think that the integrated spectroscopic technique becomes a powerful tool only in the cases where the observed objects have very small angular diameters.

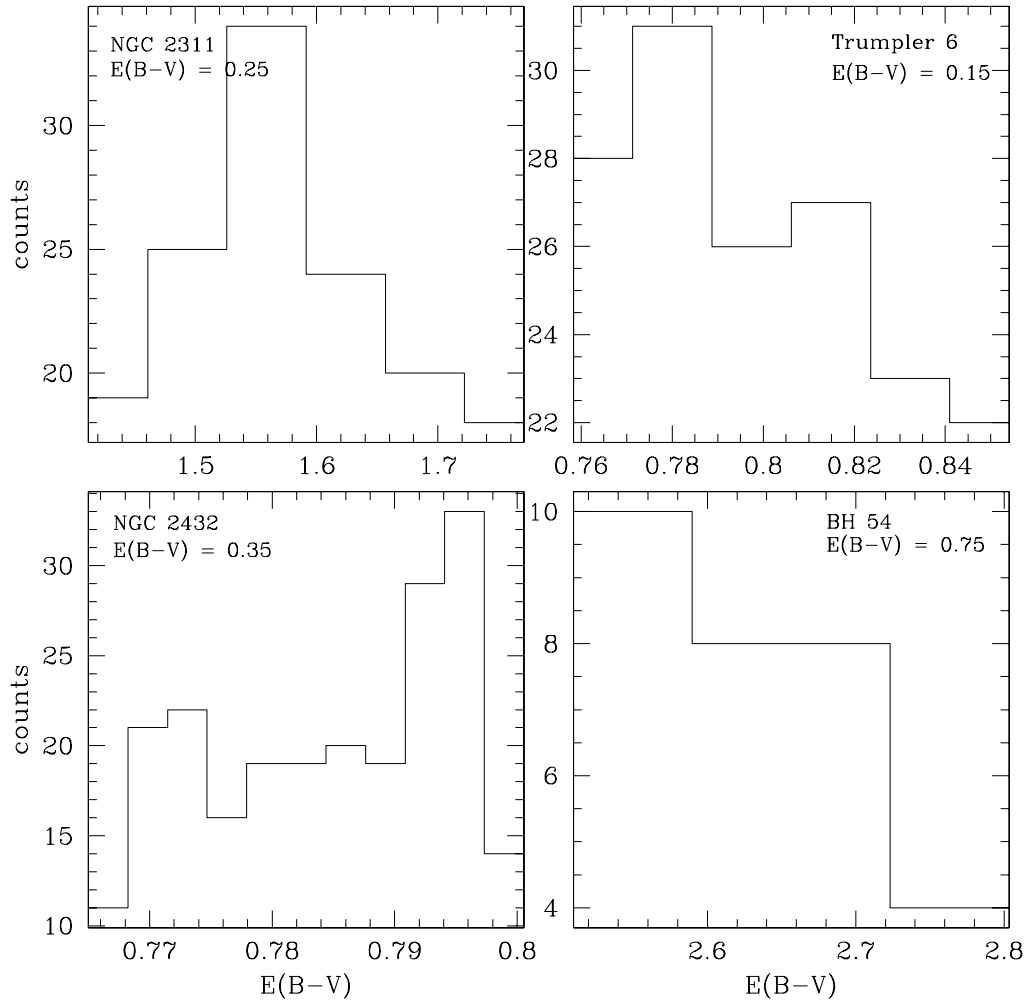

Figure 13. Histograms of the $E(B-V)$ values obtained from the SFD's 100-μm dust emission maps in the four observed fields. At the top of each panel, we include the cluster $E(B-V)$ colour excess derived in Section 4.

Table 8. Possible solutions for the fundamental parameters of the selected clusters.

	NGC 2311	Trumpler 6	NGC 2432	BH 54
$E(B-V)$ (mag)	0.25 ± 0.05	0.15 ± 0.05	0.35 ± 0.05	0.75 ± 0.05
$E(V-I)$ (mag)	0.30 ± 0.05	0.20 ± 0.05	0.45 ± 0.05	0.95 ± 0.05
$m - M_V$ (mag)	12.50 ± 0.25	10.75 ± 0.25	12.25 ± 0.25	13.00 ± 0.25
$V_o - M_V$ (mag)	11.70 ± 0.40	10.27 ± 0.40	11.13 ± 0.40	10.60 ± 0.40
d (kpc)	2.20 ± 0.40	1.10 ± 0.20	1.70 ± 0.30	1.30 ± 0.25
r (pc)	2.5 ± 0.5	0.8 ± 0.1	1.6 ± 0.3	0.6 ± 0.1
X (kpc)	10.239	9.076	9.463	8.625
Y (kpc)	−1.347	−0.934	−1.400	−1.294
Z (kpc)	−0.026	−0.070	0.053	−0.006
R_{GC} (kpc)	10.327	9.124	9.566	8.721
Age (Myr)	100^{+60}_{-40}	100^{+60}_{-40}	250^{+60}_{-50}	60^{+60}_{-30}

7 SUMMARY AND CONCLUSIONS

New CCD $UBVI_{KC}$ photometry in the field of the OCs NGC 2311, Trumpler 6, NGC 2432 and BH 54 is reported here. The analysis of the photometric data leads to the following main conclusions.

(i) Cluster CMDs cleaned from field star contamination were built by statistically subtracting the number of stars counted in the CMDs corresponding fields. Those stars closer in magnitude and colour to the ones in the respective star fields were thus removed.

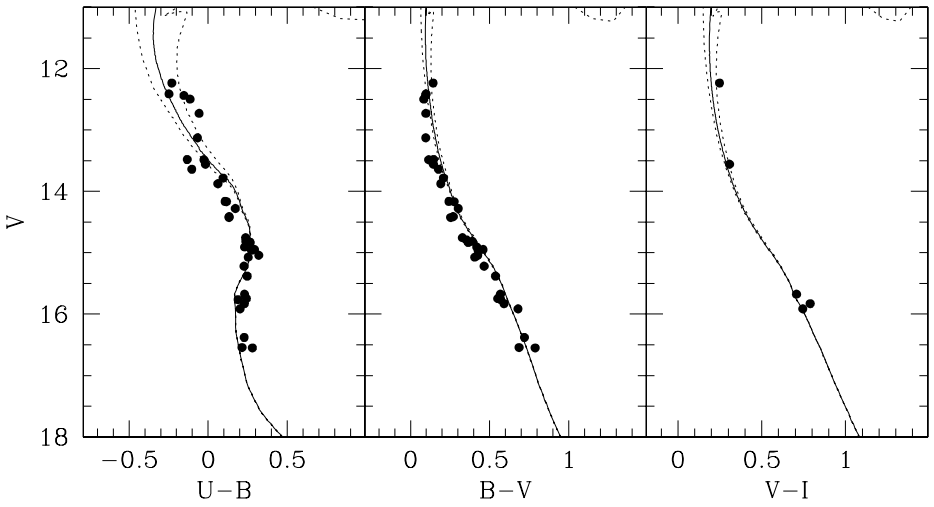

Figure 14. $(V, U-B)$, $(V, B-V)$ and $(V, V-I)$ diagrams for the probable members of NGC 2311. The adopted isochrone for $\log t = 8.0$, computed taking into account overshooting, is overplotted with solid lines. Included in dotted lines are the isochrones associated to the cluster age errors, for comparison purposes.

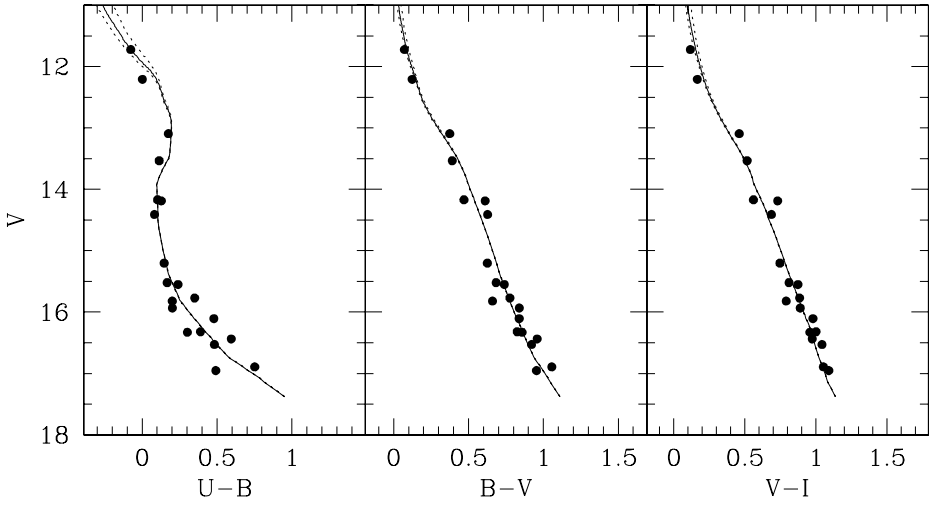

Figure 15. $(V, U-B)$, $(V, B-V)$ and $(V, V-I)$ diagrams for the probable members of Trumpler 6. The adopted isochrone for $\log t = 8.0$, computed taking into account overshooting, is overplotted with solid lines. Included in dotted lines are the isochrones associated to the cluster age errors, for comparison purposes.

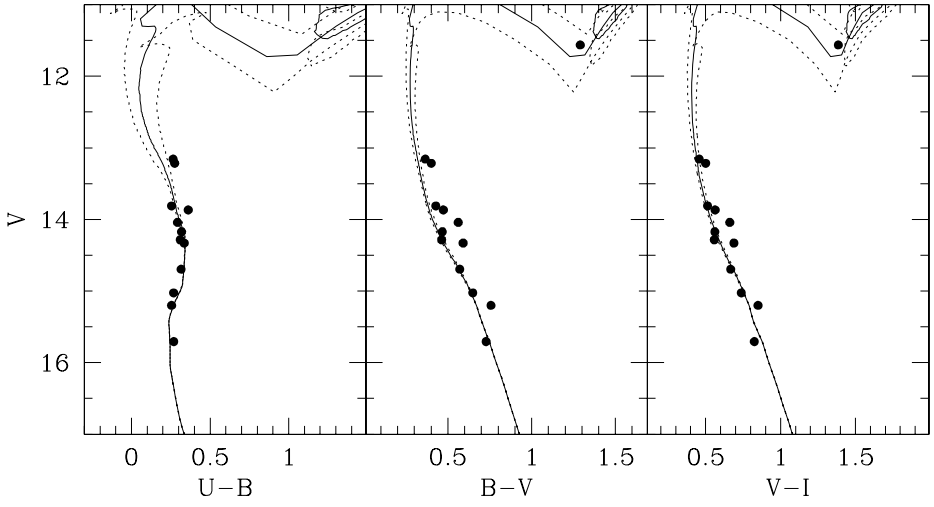

Figure 16. $(V, U-B)$, $(V, B-V)$ and $(V, V-I)$ diagrams for the probable members of NGC 2432. The adopted isochrone for $\log t = 8.40$, computed taking into account overshooting, is overplotted with solid lines. Included in dotted lines are the isochrones associated to the cluster age errors, for comparison purposes.

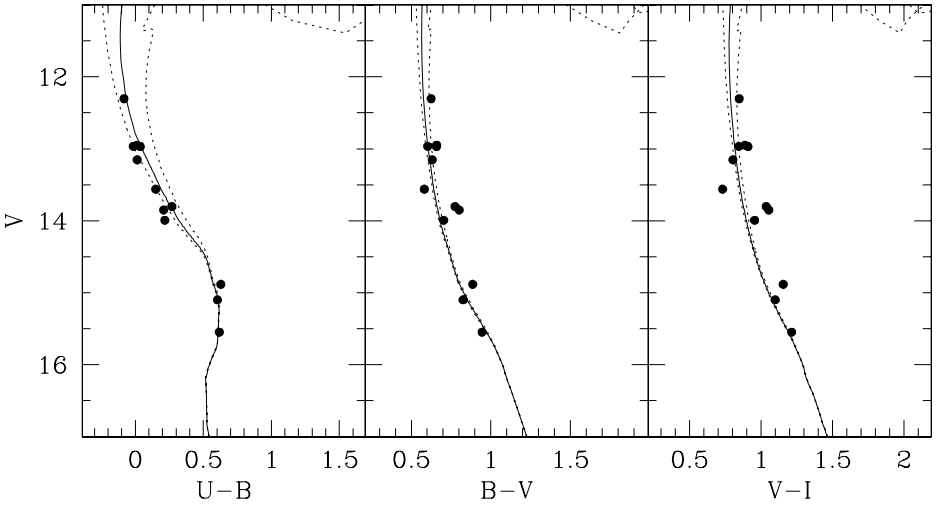

Figure 17. $(V, U-B)$, $(V, B-V)$ and $(V, V-I)$ diagrams for the probable members of BH 54. The adopted isochrone for $\log t = 7.78$, computed taking into account overshooting, is overplotted with solid lines. Included in dotted lines are the isochrones associated to the cluster age errors, for comparison purposes.

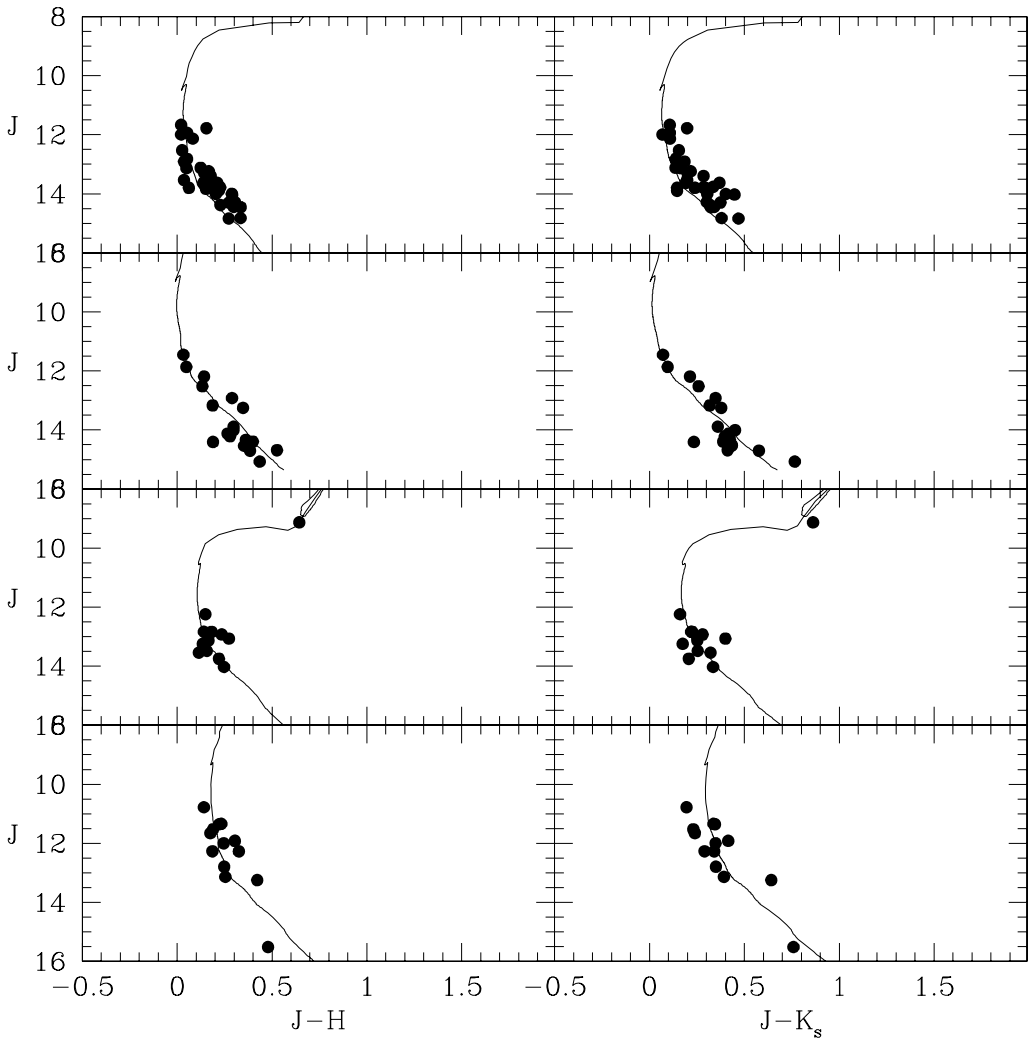

Figure 18. From top to bottom: 2MASS $(J, J-H)$ and $(J, J-K_s)$ diagrams for the probable members of NGC 2311, Trumpler 6, NGC 2432 and BH 54. The adopted isochrone from Lejeune & Schaerer (2001), computed taking into account overshooting, is overplotted with solid lines.

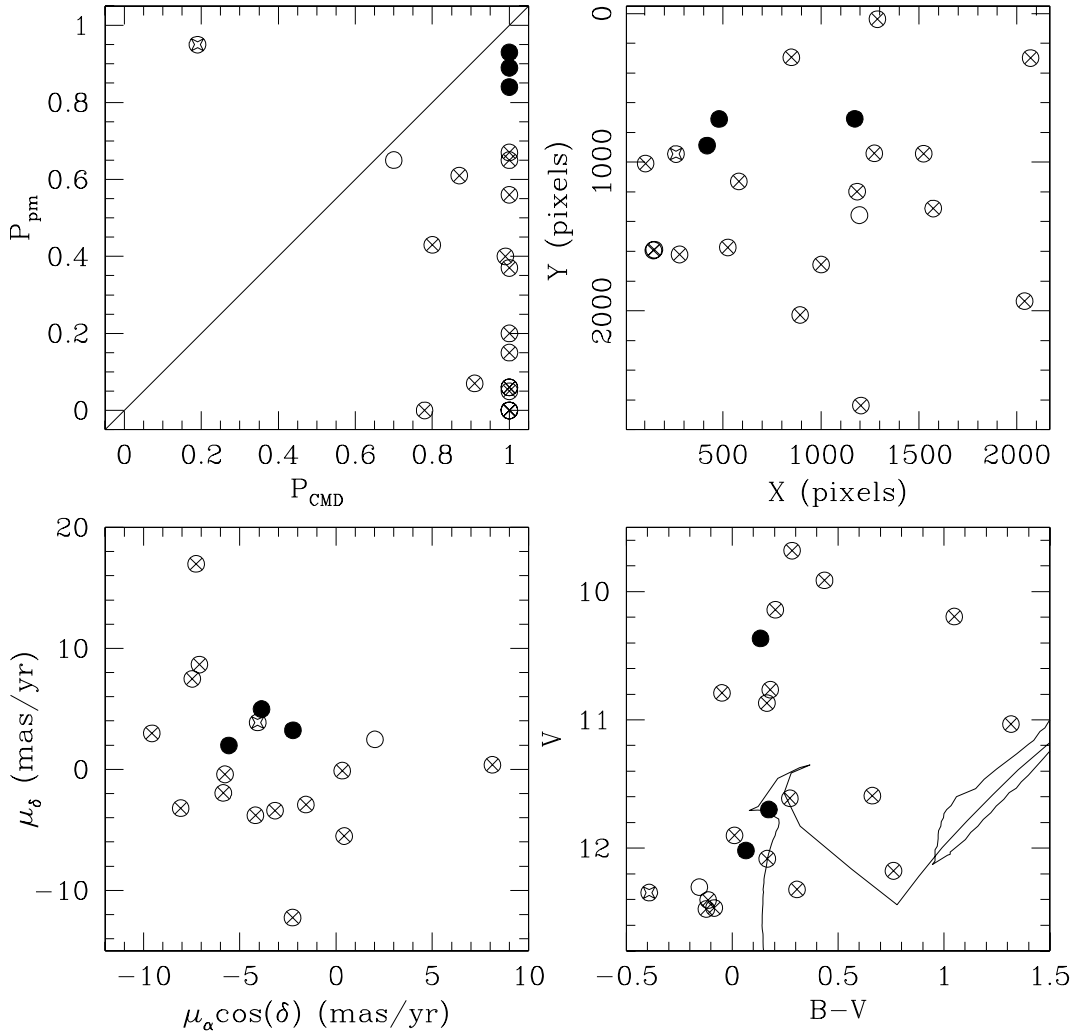

Figure 19. Relationship between different parameters derived by Kharchenko et al. (2005) for 22 stars in the field of NGC 2311. Upper left-hand panel: relation between the proper motion membership probabilities ($P_{\rm pm}$) and CMDs ($P_{\rm CMD}$) criteria; upper right-hand panel: schematic finding chart in the same coordinate system as in Fig. 1; lower left-hand panel: the proper motion plane; lower right-hand panel: ($V, B-V$) diagram with the isochrone for $t = 400$ Myr from Lejeune & Schaerer (2001) overplotted with solid line. The isochrone was shifted by $E(B-V) = 0.20$ mag and $V - M_V = 12.13$ mag. The same symbols are used in the four panels: filled circles represent stars with $P_{\rm pm}$ and $P_{\rm CMD} > 70$ per cent; crossed circles stars with $P_{\rm CMD} > 70$ per cent; starred circles stars with $P_{\rm pm} > 70$ per cent and open circles stars with $P_{\rm pm}$ and $P_{\rm CMD} < 70$ per cent.

(ii) Once the cluster centres were determined by fitting Gaussian distributions to the star counts in the x and y directions, cluster radial density profiles were built. The four studied OCs turned out to be somewhat smaller than it was previously believed.

(iii) Using the cleaned CMDs, we applied the photometric membership criteria defined by Clariá & lapasset (1986) in order to disentangle cluster member from field stars.

(iv) The interstellar extinction in the direction of the studied clusters, as measured across the cluster fields from the SFD's 100-μm dust emission full-sky maps, can be considered uniform within the quoted uncertainties.

(v) Estimates of the fundamental parameters were obtained for the cluster sample. The $E(B-V)$ and $E(V-I)$ colour excesses and the apparent distance modulus of each cluster were estimated from the fit of the ZAMS to the colour–colour and CMDs, respectively. Cluster ages were estimated by overplotting solar metallicity theoretical isochrones of the Geneva group on to the cluster CMDs. Our analysis yields $E(B-V)$ values ranging from 0.25 mag in NGC 2311 to 0.75 mag in BH 54 and heliocentric distances between 1.1 kpc (Trumpler 6) and 2.2 kpc (NGC 2311). The four studied clusters appear to be moderately young, their ages ranging between 60 and 250 Myr. Using 2MASS data, we confirmed the consistency between the 2MASS photometric scale and ours as well as our photometric membership assessment of the cluster stars.

ACKNOWLEDGMENTS

We are gratefully indebted to the CTIO staff for their hospitality and support during the observing run. This work was partially supported by the Argentinian institutions CONICET, SECYT (Universidad Nacional de Córdoba) and Agencia Nacional de Promoción Científica y Tecnológica (ANPCyT). This work is based on observations made at CTIO, which is operated by AURA, Inc., under

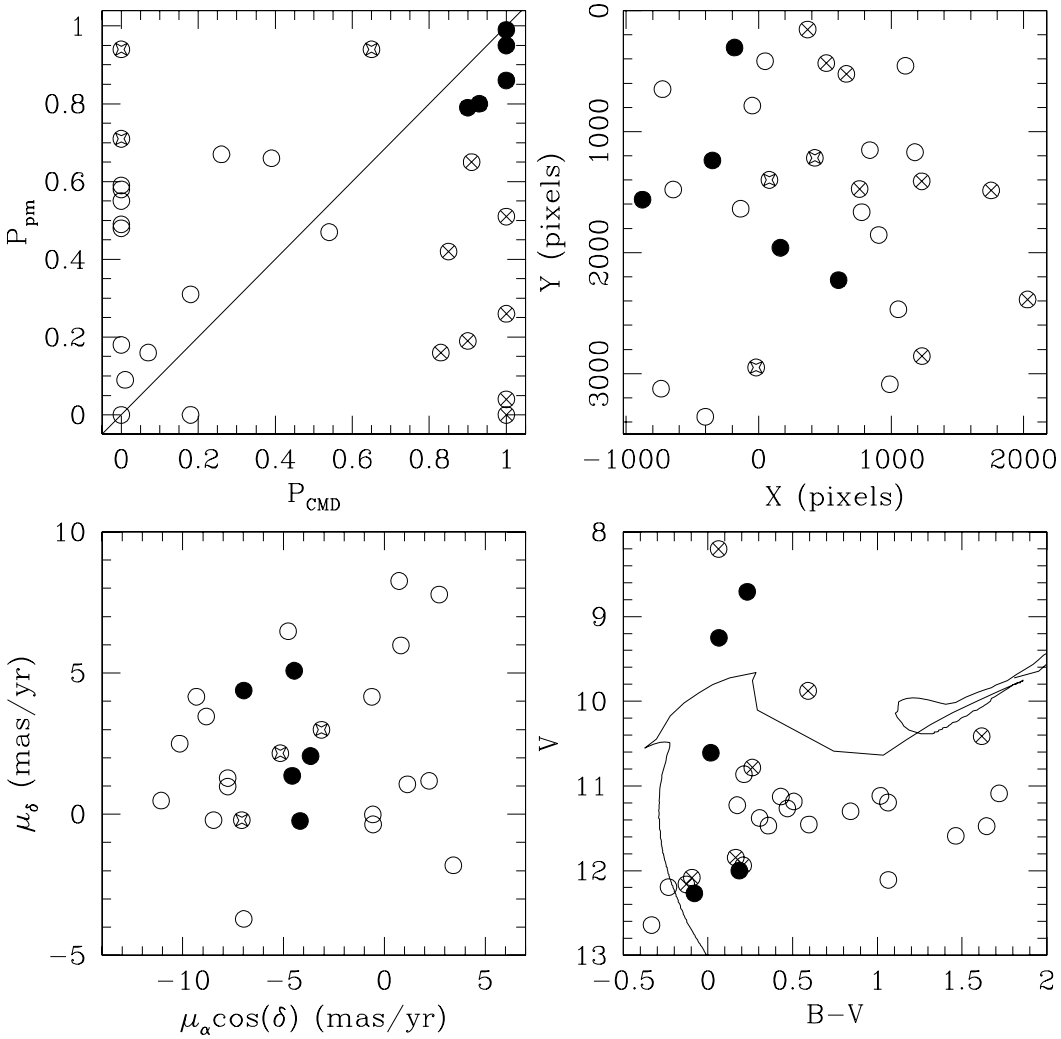

Figure 20. Same as Fig. 19 but for 30 stars in the field of NGC 2432. The isochrone for $t = 150$ Myr was shifted by $E(B-V) = 0.12$ mag and $V - M_V = 11.91$ mag.

cooperative agreement with the National Science Foundation. This research has made use of the SIMBAD data base, operated at CDS, Strasbourg, France; also the WEBDA data base, operated at the Institute for Astronomy of the University of Vienna, and the NASA's Astrophysics Data.

REFERENCES

Ahumada A. V., Clariá J. J., Bica E., 2007, A&A, 473, 437
Alter G., Ruprecht J., Vanisek J., 1970, Catalogue of Star Clusters and Associations. Akademiai Kiado, Budapest
Archinal B. A., Hynes S. J., 2003, Star Clusters. Willman-Bell, Richmond, VA
Bonatto C., Bica E., 2005, A&A, 437, 483
Bonatto C., Bica E., 2007, A&A, 473, 445
Bonatto C., Kerber L. O., Bica E., Santiago B. X., 2006, A&A, 446, 121
Burki G., Maeder A., 1973, A&A, 25, 71
Clariá J. J., Lapasset E., 1986, AJ, 91, 326
Collinder P., 1931, Medd. Lunds Astron. Obser., 2
Dean F. J., Warren P. R., Cousins A. W. J., 1978, MNRAS, 183, 569
Dutra C. M., Santiago B. X., Bica E., 2002, A&A, 383, 219
Friel E. D., 1995, ARA&A, 33, 81
Hou J.-L., Chang R.-X., Chen J. J., 2002, Chinese J. Astron. Astrophys., 1, 17
Janes K. A., Phelps R. L., 1994, AJ, 108, 1773
Kharchenko N. V., 2001, Kinematics Phys. Celest. Bodies, 17, 409
Kharchenko N. V., Piskunov A. E., Röser S., Schilbach E., Scholz R.-D., 2005, A&A, 438, 1163
Landolt A., 1992, AJ, 104, 340
Lejeune T., Schaerer D., 2001, A&A, 366, 538
Lyngå G., 1987, Catalogue of Open Cluster Data. Centre de Données Stellaires, Strasbourg
Melotte P. J., 1915, Mem. R. Astron. Soc., 60, 175
Mermilliod J.-C., Paunzen E., 2003, A&A, 410, 511
Moitinho A., 2001, A&A, 370, 436
Piatti A. E., Geisler D., Bica E., Clariá J. J., 2003, MNRAS, 343, 851
Piatti A. E., Geisler D., Sarajedini A., Gallart C., Wischnjewsky M., 2008, MNRAS, 389, 429
Piatti A. E., Clariá J. J., Ahumada A. V., 2009, MNRAS, 397, 1073
Piskunov A. E., Kharchenko N. V., Roser S., Schilbach E., Scholz R. D., 2006, A&A, 445, 545
Schlegel D. J., Finkbeiner D. P., Davis M., 1998, ApJ, 500, 525 (SFD)
Skrutskie M. F. et al., 2006, AJ, 131, 1163
Straizys V., 1992, Multicolor Stellar Photometry. Pachart Publishing House, Tucson, AZ

Trumpler R. J., 1930, Lick Obser. Bull., 14, 154
Turner D. G., 1994, Revista Mexicana Astron. Astrofisica, 29, 163
van den Bergh S., Hagen G. L., 1975, AJ, 80, 11

SUPPORTING INFORMATION

Additional Supporting Information may be found in the online version of this article:

Table 4. CCD *UBVI* data for stars in the field of NGC 2311.
Table 5. CCD *UBVI* data for stars in the field of Trumpler 6.
Table 6. CCD *UBVI* data for stars in the field of NGC 2432.
Table 7. CCD *UBVI* data for stars in the field of BH 54.

Please note: Wiley-Blackwell are not responsible for the content or functionality of any supporting materials supplied by the authors. Any queries (other than missing material) should be directed to the corresponding author for the article.

This paper has been typeset from a TEX/LATEX file prepared by the author.